

# Probing TeV-Scale Inverse-Seesaw Leptogenesis and Majorana Dark Matter in $U(1)_{B-L}$ Models at Multi-TeV Muon Colliders

Xin-Qiang Li <sup>a</sup>, Himadri Roy <sup>a</sup>, Tripurari Srivastava <sup>a</sup>, Ya-Dong Yang <sup>a,c</sup> and Xing-Bo Yuan <sup>a</sup>

<sup>a</sup>*Institute of Particle Physics and Key Laboratory of Quark and Lepton Physics (MOE), Central China Normal University, Wuhan, Hubei 430079, China*

<sup>c</sup>*Institute of Particle and Nuclear Physics, Henan Normal University, Xinxiang 453007, China*

*E-mail:* [xqli@mail.ccnu.edu.cn](mailto:xqli@mail.ccnu.edu.cn), [himadri027roy@gmail.com](mailto:himadri027roy@gmail.com), [tripurari.sri022@gmail.com](mailto:tripurari.sri022@gmail.com), [yangyd@mail.ccnu.edu.cn](mailto:yangyd@mail.ccnu.edu.cn), [y@ccnu.edu.cn](mailto:y@ccnu.edu.cn)

**ABSTRACT:** We investigate a predictive and testable framework in which dark matter (DM), heavy-neutrino dynamics, and the baryon asymmetry of the Universe originate from correlated interactions within a local  $U(1)_{B-L}$  extension of the Standard Model. Unlike conventional  $B-L$  constructions based on the type-I seesaw, we employ an inverse-seesaw mechanism realized through a sterile fermion  $S_1$  and a complex scalar field  $\phi$ , whose vacuum expectation value simultaneously generates the masses of the heavy neutrinos  $N_{1,2}$  and the Majorana DM fermion  $\chi$  via Yukawa couplings. The small lepton-number-violating parameter induced by a higher-dimensional operator leads to naturally light active neutrinos together with TeV-scale heavy neutrinos and sizable active-sterile mixing, yielding distinctive collider signatures unavailable in minimal  $B-L$  models. The relic abundance of  $\chi$  is governed by annihilation channels mediated by the same scalar and gauge interactions, producing a direct and model-specific correlation between successful leptogenesis and the observed DM relic density. A combined parameter-space analysis incorporating neutrino oscillation data, lepton-flavor-violating processes, direct-detection limits, and collider bounds on  $N_{1,2}$  and  $Z'$  reveals a narrow yet robust region consistent with all these constraints. Representative benchmark points in this region are examined at a future multi-TeV muon collider. Heavy-neutrino production through electroweak processes yields striking signatures in the dilepton plus missing energy ( $2\ell + \cancel{E}_T$ ) and single-lepton plus di-jet plus missing energy ( $1\ell + 2j + \cancel{E}_T$ ) final states. These channels demonstrate that next-generation muon colliders offer a powerful and complementary probe of the inverse-seesaw origin of neutrino masses, the DM relic density, and the TeV-scale leptogenesis within such an extended  $U(1)_{B-L}$  framework.

**KEYWORDS:** Specific BSM Phenomenology, Dark Matter at Colliders, Sterile or Heavy Neutrinos

---

## Contents

<b>1</b>	<b>Introduction</b>	<b>1</b>
<b>2</b>	<b>Theoretical Framework</b>	<b>3</b>
<b>3</b>	<b>Phenomenological Constraints</b>	<b>4</b>
3.1	Neutrino Mass Fitting	4
3.2	LFV Constraints	5
3.3	Leptogenesis	5
3.4	Dark Matter	7
<b>4</b>	<b>Boltzmann Evolution</b>	<b>8</b>
<b>5</b>	<b>Numerical Analysis</b>	<b>10</b>
<b>6</b>	<b>Collider Phenomenology</b>	<b>13</b>
6.1	Dilepton Final State $2\ell + \cancel{E}_T$	14
6.2	$1\ell + 2j + \cancel{E}_T$ Final State	18
<b>7</b>	<b>Conclusion</b>	<b>23</b>

---

## 1 Introduction

The discovery of the Higgs boson at the Large Hadron Collider (LHC) [1, 2] has completed the particle spectrum of the Standard Model (SM) and confirmed the mechanism of electroweak symmetry breaking that endows fermions and gauge bosons with masses [3–6]. Despite the tremendous success, several fundamental questions remain unanswered within the SM framework. A striking example is the origin of tiny but non-zero neutrino masses, strongly supported by neutrino oscillation experiments [7, 8] and constrained by cosmology to satisfy  $\sum m_\nu < 0.12$  eV [9]. Since neutrinos are massless in the SM, this observation provides unambiguous evidence for new physics (NP) beyond the SM.

A minimal and widely studied possibility for generating neutrino masses is the type-I seesaw mechanism [10–13], in which heavy right-handed neutrinos generate suppressed Majorana masses for active neutrinos. However, in its conventional form, the type-I seesaw mechanism typically requires large Majorana masses or tiny Yukawa couplings, leading to active–sterile mixing angles far below the sensitivity of current colliders [14, 15]. To obtain testable TeV-scale heavy neutrinos while retaining naturally small neutrino masses, extensions of the fermion sector, such as the inverse-seesaw mechanism, are well motivated [16–24], where small lepton-number–violating (LNV) parameters, rather than ultra-heavy mass scales, account for the lightness of active neutrinos [25–31].

In addition to the non-vanishing neutrino masses, the observed baryon asymmetry of the Universe (BAU) [9],

$$\eta_B = \frac{n_B - n_{\bar{B}}}{n_\gamma} \simeq 6.12 \times 10^{-10}, \quad (1.1)$$

cannot be generated within the SM, which lacks sufficient CP violation and the necessary out-of-equilibrium dynamics. Leptogenesis [32–46], in which heavy Majorana neutrinos produce a lepton asymmetry that is later converted to a baryon asymmetry by sphaleron processes [32, 47–53], provides an elegant explanation. Standard thermal leptogenesis [54] typically operates at very high scales, but in scenarios with quasi-degenerate heavy neutrinos, particularly relevant for the inverse-seesaw mechanism, a resonant enhancement [35, 55–60] of CP violation allows successful leptogenesis at the TeV scale [35, 55–58, 61–64]. Another major shortcoming of the SM is its inability to account for dark matter (DM) [65, 66], which constitutes about 27% of the energy density of the Universe according to *Planck* [67]. Thus, models linking DM with the origin of neutrino masses are especially appealing, as they address two seemingly unrelated problems within a unified framework [25–31].

A simple and well-motivated extension of the SM that naturally connects neutrino masses, DM, and baryogenesis is the introduction of a local  $U(1)_{B-L}$  gauge symmetry [68–70]. Spontaneous breaking of this symmetry generates the Majorana masses required for the seesaw mechanism, introduces a massive  $Z'$  gauge boson, and can leave behind a residual discrete symmetry (such as a  $\mathbb{Z}_2$  symmetry) that stabilizes the DM particle [71–73]. In such a framework, the interactions responsible for generating neutrino masses also play a central role in DM annihilation processes and in producing a baryon asymmetry [74–76]. The TeV-scale realization of the  $U(1)_{B-L}$  model is particularly attractive: both the heavy neutrinos and the  $Z'$  boson can lie within the reach of the collider, while the same gauge and Yukawa interactions control DM freeze-out and leptogenesis [71–76].

In this work, we study an extended  $U(1)_{B-L}$  inverse-seesaw model that successfully explains the neutrino mass scale, the baryon asymmetry through resonant leptogenesis, and the DM relic abundance. The model contains two right-handed neutrinos, two gauge-singlet fermions, and a complex scalar whose vacuum expectation value (VEV) breaks the  $B - L$  symmetry. The resulting heavy neutrinos and the DM particle naturally reside at the TeV scale, establishing a tight connection between cosmological dynamics and collider phenomenology [60–64]. We further analyze the collider signatures associated with the production of heavy neutrinos and the  $Z'$  boson at future high-energy muon colliders. Such facilities provide a clean environment in which the small but non-negligible active–sterile mixing of the inverse seesaw can still yield observable leptonic and semi-leptonic final states (see, e.g., Refs. [61–64] for related studies). Using a cut-based analysis for several benchmark points consistent with cosmological constraints, we will examine the discovery prospects at future high-energy muon colliders with  $\sqrt{s} = 6$  and 10 TeV [77].

The paper is organized as follows. Section 2 introduces our theoretical setup and the field content of the model. In section 3, we present the phenomenological constraints on the model, including neutrino mass fitting, lepton-flavor violation, leptogenesis, and the DM relic abundance. Section 4 describes the Boltzmann evolution equations that govern the dynamics of heavy neutrinos, DM, and the  $B - L$  asymmetry. The numerical analysis

of the viable parameter space is presented in section 5. In section 6, we explore the collider phenomenology at a multi-TeV muon collider, focusing on the most relevant leptonic and semi-leptonic final states. Finally, in section 7 we summarize our main results and discuss the broader implications for future experimental tests of such a unified  $U(1)_{B-L}$  framework.

## 2 Theoretical Framework

The model we are considering here is based on the extended gauge symmetry

$$SU(2)_L \otimes U(1)_Y \otimes U(1)_{B-L} \otimes \mathbb{Z}_2, \quad (2.1)$$

and extends the SM by a complex scalar singlet  $\phi$  that spontaneously breaks  $U(1)_{B-L}$ , a set of gauge-singlet fermions  $(N, S_1)$ , and a fermionic DM candidate  $\chi$ . The  $\mathbb{Z}_2$  symmetry is imposed to stabilize the dark sector:  $\chi$  is  $\mathbb{Z}_2$ -odd, while all SM fields and the remaining new fields are  $\mathbb{Z}_2$ -even. The field content and charge assignments under  $(SU(2)_L, U(1)_Y, U(1)_{B-L}, \mathbb{Z}_2)$  are listed as

$$\begin{aligned} q_L(2, +\frac{1}{6}, +\frac{1}{3}, +), & \quad u_R(1, +\frac{2}{3}, +\frac{1}{3}, +), & \quad d_R(1, -\frac{1}{3}, +\frac{1}{3}, +), \\ L_L(2, -\frac{1}{2}, -1, +), & \quad e_R(1, -1, -1, +), & \quad N(1, 0, -1, +), \\ H(2, +\frac{1}{2}, 0, +), & \quad \phi(1, 0, +2, +), \\ S_1(1, 0, +1, +), & \quad \chi(1, 0, -1, -), \end{aligned} \quad (2.2)$$

where the  $\mathbb{Z}_2$ -odd assignment of  $\chi$  forbids all its decays into lighter  $\mathbb{Z}_2$ -even states, ensuring its stability on cosmological time scales. This construction is inspired by the study in Ref. [68], but with an extended singlet-fermion sector arranged to realize the inverse-seesaw mechanism [16–24].

The gauge-invariant Yukawa sector relevant for neutrino masses and DM mass generation is given by<sup>1</sup>

$$\mathcal{L} \supset -y_\nu \bar{L}_L \tilde{H} N - M \bar{N}^c S_1 - \frac{\lambda_\mu}{\sqrt{2}} \phi^\dagger \bar{S}_1^c S_1 - \frac{\lambda_\chi}{\sqrt{2}} \phi \bar{\chi}^c \chi + \text{h.c.}, \quad (2.3)$$

where  $\tilde{H} \equiv i\sigma_2 H^*$  and  $\psi^c \equiv C\bar{\psi}^T$ , with  $\sigma_2$  and  $C$  denoting the second Pauli matrix and the charge-conjugation operator, respectively. The first term generates the Dirac mass  $m_D = y_\nu v_H/\sqrt{2}$  after electroweak symmetry breaking. The second term provides a large lepton-number-conserving singlet mass scale  $M$  that links  $N$  and  $S_1$ . The third term induces a small LNV parameter  $\mu = \lambda_\mu v_\phi/2$  once  $U(1)_{B-L}$  is broken by  $\langle \phi \rangle = v_\phi/\sqrt{2}$ . Finally, the last term generates the DM mass  $m_\chi = \lambda_\chi v_\phi/2$  and, together with the  $\mathbb{Z}_2$  symmetry, ensures the stability of  $\chi$ .

---

<sup>1</sup>Although the operator  $\phi \bar{N}^c N$  is allowed by the gauge symmetry, it can be forbidden by an additional symmetry acting on the sterile-fermion sector. For example, one may impose a lepton-number-like global symmetry under which the  $\bar{N}^c N$  Majorana term is not invariant, while the Dirac-type term  $\bar{N}^c S_1$  and the small  $\mu$  term in the  $S_1$  sector are retained. Here we effectively assume this symmetry, so that the heavy sterile states form a pseudo-Dirac pair and the neutrino mass matrix retains the inverse-seesaw structure.

The scalar sector contains the SM Higgs doublet  $H$  and the  $B - L$ -breaking singlet  $\phi$ , with VEVs given by  $\langle H \rangle = v_H/\sqrt{2}$  and  $\langle \phi \rangle = v_\phi/\sqrt{2}$  respectively, where  $v_H = 246$  GeV. The renormalizable potential involving these fields reads

$$V(H, \phi) = -\mu_H^2 H^\dagger H - \mu_\phi^2 \phi^\dagger \phi + \lambda_H (H^\dagger H)^2 + \lambda_\phi (\phi^\dagger \phi)^2 + \lambda_{H\phi} (H^\dagger H)(\phi^\dagger \phi). \quad (2.4)$$

Minimization of  $V$  gives

$$\mu_H^2 = \lambda_H v_H^2 + \frac{1}{2} \lambda_{H\phi} v_\phi^2, \quad \mu_\phi^2 = \lambda_\phi v_\phi^2 + \frac{1}{2} \lambda_{H\phi} v_H^2, \quad (2.5)$$

and the physical spectrum contains one CP-odd scalar  $\eta$  corresponding to the imaginary component of  $\phi$ , as well as two CP-even scalars  $h$  and  $\rho$  obtained from the mixing of the neutral Higgs component and the real part of  $\phi$ . Here  $h$  is identified as the SM Higgs boson, and the mixing angle is denoted by  $\theta$ .

### 3 Phenomenological Constraints

In this section, we examine the main constraints that shape the viable parameter space of the model. These include the requirement of correctly reproducing the observed neutrino mass and mixing pattern, the bounds from LFV decays, the conditions needed for successful leptogenesis, and the DM relic-density limits. Each of these constraints probes a different part of the Yukawa couplings, masses, and mixings in the model; taken together, they determine the region in which the model remains consistent with current data. We discuss these aspects in the following subsections.

#### 3.1 Neutrino Mass Fitting

After spontaneous breaking of the electroweak and  $U(1)_{B-L}$  symmetries, the Yukawa interactions in Eq. (2.3) give rise to neutrino mass terms involving the left-handed SM neutrinos  $\nu_L$  and the gauge-singlet fermions  $N$  and  $S_1$ . The relevant mass Lagrangian can be written as

$$\mathcal{L}_m^\nu = m_D \bar{\nu}_L N + M \bar{N}^c S_1 + \mu \bar{S}_1^c S_1 + \text{h.c.}, \quad (3.1)$$

where the Dirac and singlet mass matrices are given, respectively, by

$$m_D = y_\nu \frac{v_H}{\sqrt{2}}, \quad M \equiv M_{NS}, \quad \mu = \lambda_\mu \frac{v_\phi}{2}. \quad (3.2)$$

Here  $v_H$  and  $v_\phi$  denote the VEVs of the SM Higgs doublet and the  $B - L$ -breaking scalar  $\phi$ , respectively. The parameter  $\mu$  originates from the gauge-invariant interaction  $\phi^\dagger \bar{S}_1^c S_1$ , and softly violates lepton number after  $U(1)_{B-L}$  breaking.

In the flavor basis

$$\psi^T = (\nu_L, N^c, S_1), \quad (3.3)$$

the complete neutrino mass matrix takes the characteristic inverse-seesaw form

$$\mathcal{M}_\nu = \begin{pmatrix} 0 & m_D & 0 \\ m_D^T & 0 & M \\ 0 & M^T & \mu \end{pmatrix}. \quad (3.4)$$

In the phenomenologically relevant limit

$$\|\mu\| \ll \|M\|, \quad \|m_D\| \ll \|M\|, \quad (3.5)$$

the effective light-neutrino mass matrix obtained by block diagonalization reads

$$m_\nu \simeq m_D M^{-1} \mu (M^{-1})^T m_D^T, \quad (3.6)$$

which demonstrates that the smallness of the active neutrino masses is controlled by the LNV parameter  $\mu$ , rather than by an ultra-heavy seesaw scale  $M$ . As a result, all singlet fermions can naturally reside at the TeV scale, while remaining compatible with the sub-eV neutrino masses required by neutrino oscillation data [78].

The heavy neutral-fermion spectrum consists of two quasi-degenerate Majorana states per generation, with masses given approximately by

$$m_{\nu_H}^2 \simeq M^2 + m_D^2, \quad (3.7)$$

up to a small splitting of  $\mathcal{O}(\mu)$ . The hierarchy

$$m_\nu \ll m_D \ll M, \quad (3.8)$$

together with the smallness of  $\mu$ , ensures moderately large active–sterile mixing, while keeping the heavy states nearly degenerate. This quasi-degeneracy plays a crucial role in the resonant enhancement of CP violation in low-scale leptogenesis, and will be exploited in the phenomenological analysis presented in the latter sections.

### 3.2 LFV Constraints

The flavor mixing in the neutrino sector leads to LFV processes at one loop, such as  $\mu \rightarrow e\gamma$  [79],  $\tau \rightarrow e\gamma$  [80], and  $\tau \rightarrow \mu\gamma$  [80], as well as the three-body decays  $\mu \rightarrow eee$  and  $\tau \rightarrow \ell\ell\ell$ , with  $\ell = e, \mu$ . The fact that none of these processes has yet been observed so far puts strong bounds on their branching ratios. These bounds restrict the allowed parameter space in the neutrino sector of the model. We compute the contributions to the LFV processes and use the experimental limits to constrain the model.

### 3.3 Leptogenesis

In our framework, the decay of heavy Majorana neutrinos  $N_i$  plays a crucial role in the generation of the BAU [47, 81, 82]. The Yukawa interactions characterized by the coupling  $y_\nu$  in Eq. (2.3) permit the out-of-equilibrium decays

$$N_i \rightarrow L_\alpha H, \quad N_i \rightarrow \bar{L}_\alpha H^*, \quad (3.9)$$

where  $L_\alpha$  represents the lepton doublet and  $H$  is the SM Higgs field. When the Yukawa coupling  $y_\nu$  contains complex phases, these processes can violate CP symmetry, resulting in a small difference between the decay rates of a neutrino and its CP-conjugate channel [83]. The CP asymmetry parameter associated with the decays of  $N_i$  is defined by

$$\epsilon_i = \frac{\sum_j \Gamma(N_i \rightarrow L_\alpha H) - \Gamma(N_i \rightarrow \bar{L}_\alpha H^*)}{\sum_j \Gamma(N_i \rightarrow L_\alpha H) + \Gamma(N_i \rightarrow \bar{L}_\alpha H^*)}, \quad (3.10)$$

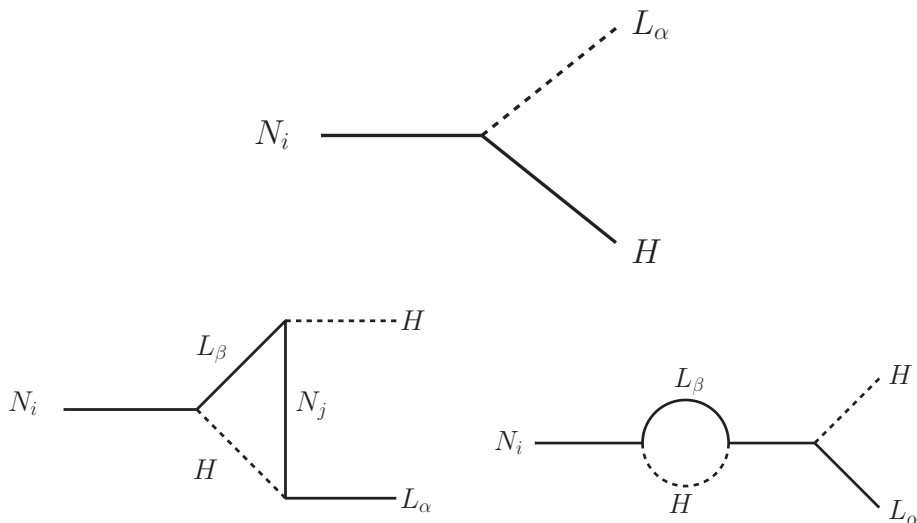


**Figure 1.** Feynman diagrams contributing to the CP-violating decays of heavy Majorana neutrinos. The top diagram shows the tree-level process  $N_i \rightarrow L_\alpha H$ , while the bottom diagrams represent the one-loop vertex and self-energy corrections mediated by virtual heavy neutrino states  $N_j$ , whose interference with the tree-level amplitude generates the CP asymmetry  $\epsilon_i$ .

which follows the standard treatment in thermal leptogenesis [83–87].

The decay amplitude of  $N_i \rightarrow L_\alpha H$  receives contributions from both the tree-level diagram as well as the one-loop vertex and self-energy corrections, as depicted in Fig. 1. The interference between these diagrams generates a nonvanishing  $\epsilon_i$  [47]. In the type-I seesaw picture, the total CP asymmetry arising from these interferences is given by

$$\epsilon_i = - \sum_{j \neq i} \frac{M_{N_i} \Gamma_{N_j}}{M_{N_j}^2} \frac{\text{Im}[(y_\nu y_\nu^\dagger)_{ij}^2]}{(y_\nu y_\nu^\dagger)_{ii} (y_\nu y_\nu^\dagger)_{jj}} \left\{ x_{ij} \left[ (1 + x_{ij}) \ln \left( 1 + \frac{1}{x_{ij}} \right) - 1 \right] + \frac{x_{ij}(x_{ij} - 1)}{(x_{ij} - 1)^2 + (\Gamma_{N_j}/M_{N_i})^2} \right\}, \quad (3.11)$$

where  $x_{ij} = M_{N_j}^2/M_{N_i}^2$ , and  $\Gamma_{N_j}$  denotes the total decay width of the heavy neutrino  $N_j$  [57, 88–90]. The first term within the brackets originates from the vertex correction, while the second term represents the self-energy (wave-function) contribution.

In the case where the heavy-neutrino mass spectrum is nearly degenerate,

$$\left| M_{N_j}^2 - M_{N_i}^2 \right| \simeq M_{N_i} \Gamma_{N_j}, \quad (3.12)$$

the self-energy term in Eq. (3.11) experiences a resonant enhancement [58, 91, 92]. Consequently, the CP asymmetry  $\epsilon_i$  can become of order unity, even when the Yukawa couplings are relatively small. This phenomenon, known as *resonant leptogenesis* [56, 93–95], enables the generation of the observed BAU at the TeV scale – much lower than the scale required by traditional high-scale thermal leptogenesis.

The asymmetry produced in the decays of  $N_i$  is subsequently converted into a net baryon asymmetry through  $B + L$ -violating sphaleron transitions that remain active above the electroweak phase transition temperature [50–52]. In this scenario, the interplay between the small mass splitting among the heavy neutrinos and the complex structure of  $y_\nu$  determines the magnitude of the CP asymmetry, ensuring successful low-scale leptogenesis consistent with the current experimental data [81, 96].

### 3.4 Dark Matter

The fermionic field  $\chi$  serves as the DM candidate in our framework. Its stability is ensured by an imposed discrete  $\mathbb{Z}_2$  symmetry, under which  $\chi$  is odd, while all SM particles remain even. This discrete charge assignment forbids any renormalizable interaction that could induce its decay into SM states, thereby guaranteeing the cosmological longevity of  $\chi$ .

To investigate the DM phenomenology, we evaluate the relic abundance of  $\chi$  and confront it with the observed DM relic density determined by the *Planck* collaboration [65–67]. The numerical analysis is performed using the `micrOMEGAs` package [97], which computes the thermal relic density by solving the Boltzmann equation, including all relevant annihilation and coannihilation channels. The results are further constrained using the latest direct-detection limits reported by the LUX-ZEPLIN (LZ-2024) experiment [98], ensuring that the parameter space remains consistent with the existing observational data.

The main annihilation processes that contribute to the thermal freeze-out of  $\chi$  are illustrated in Fig. 2. The most significant channels can be summarized as follows [68]:

- Annihilation of  $\chi\chi$  into a pair of singlet scalars  $\eta\eta$  through the  $s$ -channel exchange of the scalar mediator  $\rho(h)$ .
- Annihilation of  $\chi\chi$  into two scalar mediators  $\rho(h)\rho(h)$  through the  $t$ -channel exchange of  $\chi$ .
- Annihilation of  $\chi\chi$  or  $N_i N_i$  into  $\rho(h)\rho(h)$  through the  $t$ -channel exchange of  $\chi$ .
- Annihilation of  $\chi\chi$  or  $N_i N_i$  into  $Z'Z'$  through the  $t$ -channel exchange of  $\chi$ .
- Annihilation of  $\chi\chi$  into SM particles or sterile neutrinos  $N$  through the  $s$ -channel exchange of  $\rho(h)$ .
- Annihilation of  $\chi\chi$  into SM particles or sterile neutrinos  $N$  through the  $s$ -channel exchange of the gauge boson  $Z'$ .
- Annihilation of  $\chi\chi$  or  $N_i N_i$  into  $Z'Z'$  through the  $s$ -channel exchange of  $\rho(h)$ .
- Annihilation of  $\chi\chi$  or  $N_i N_i$  into  $\rho(h)\rho(h)$  through the  $s$ -channel exchange of  $\rho(h)$ .

In this analysis, the mass of  $\chi$  is taken to lie above the electroweak scale to avoid the experimental limits on the invisible Higgs decay width. This mass range also allows  $\chi$  to achieve the correct relic density through thermal freeze-out, governed primarily by the interplay between the scalar and gauge portal interactions described above.

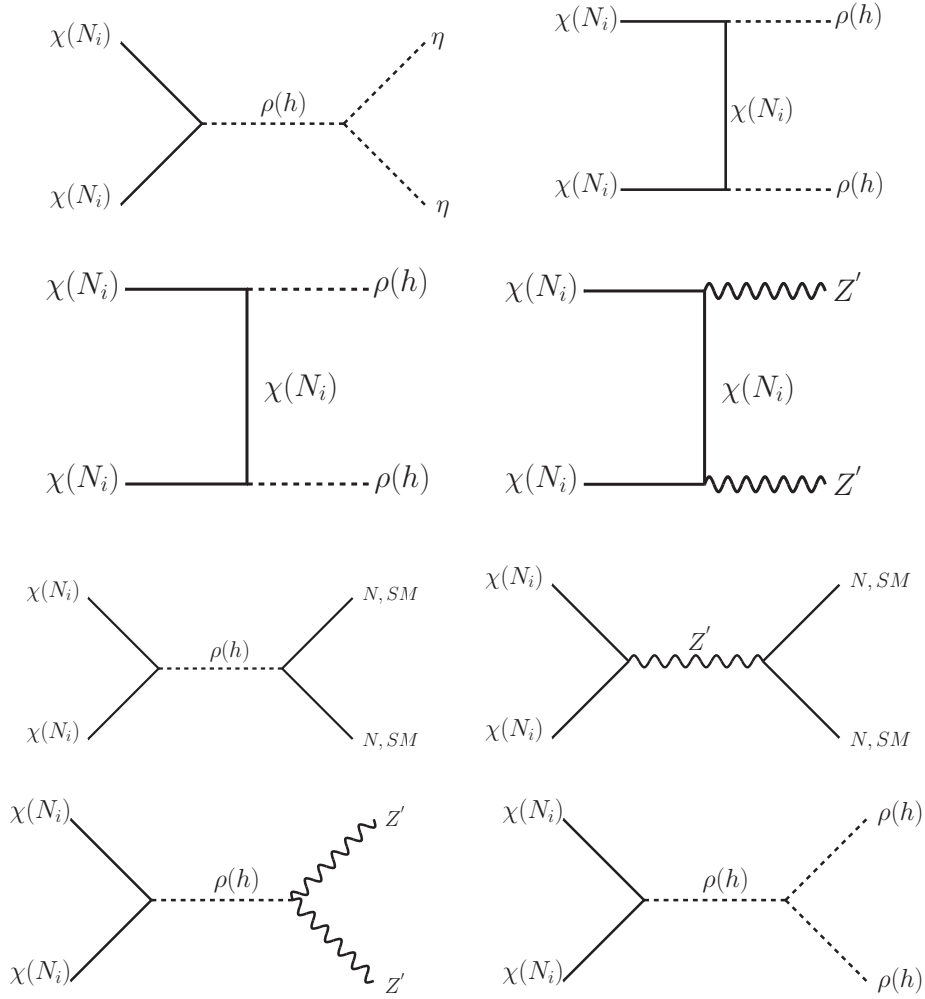


**Figure 2.** Representative annihilation diagrams of the DM particle  $\chi$ . These include interactions mediated by the scalar fields  $\eta$ ,  $\phi$ , and by the  $U(1)_{B-L}$  gauge boson  $Z'$ , as well as the mixed annihilation channels with heavy neutrinos. The relic density and freeze-out behavior of  $\chi$  are governed by these dominant processes.

The viable parameter space consistent with the observed DM relic abundance and direct-detection bounds typically corresponds to moderate Yukawa couplings and a  $Z'$  mass of order a few TeV. These conditions ensure that the model remains perturbative and compatible with current collider and cosmological constraints, while simultaneously providing a compelling unified framework for neutrino mass generation and DM stability [74, 76].

#### 4 Boltzmann Evolution

The cosmological evolution of the heavy Majorana neutrinos  $N_i$ , the DM fermion  $\chi$ , and the generated  $B-L$  asymmetry is described by a coupled system of Boltzmann equations [47, 74, 76, 81, 99]. These equations govern the evolution of the comoving number densities  $Y_X \equiv n_X/s$ , where  $n_X$  is the number density of a given particle species and  $s$  denotes the

entropy density of the Universe. The temperature dependence is expressed in terms of the dimensionless variable  $z = m_{N_1}/T$ , with  $T$  being the plasma temperature. The expansion of the Universe is characterized by the Hubble parameter  $H$ , evaluated at the relevant temperature scale.

The evolution equations for  $Y_{N_i}$ ,  $Y_\chi$ , and the net  $B - L$  asymmetry  $Y_{B-L}$  are given, respectively, by [68]

$$\begin{aligned} \frac{dY_{N_i}}{dz} = & -\frac{z}{sH(m_{N_1})} \left( \frac{Y_{N_i}}{Y_{N_i}^{\text{eq}}} - 1 \right) \left( \gamma_{N_i \rightarrow \ell H} + 2\gamma_{N_i \ell \rightarrow qt} + 4\gamma_{N_i t \rightarrow ql} \right) \\ & - \frac{z}{sH(m_{N_1})} \left[ \left( \frac{Y_{N_i}}{Y_{N_i}^{\text{eq}}} \right)^2 - 1 \right] \left( 2\gamma_{N_i N_i \rightarrow \rho\rho, Z'Z'} + 2\gamma_{N_i N_i \rightarrow \rho Z', hZ'} + 2\gamma_{N_i N_i \rightarrow \text{SM}} \right) \\ & + \frac{z}{sH(m_{N_1})} \left[ \left( \frac{Y_\chi}{Y_\chi^{\text{eq}}} \right)^2 - \left( \frac{Y_{N_i}}{Y_{N_i}^{\text{eq}}} \right)^2 \right] 2\gamma_{\chi\chi \rightarrow N_i N_i}, \end{aligned} \quad (4.1)$$

$$\begin{aligned} \frac{dY_\chi}{dz} = & - \sum_{i=1,2} \frac{z}{sH(m_{N_1})} \left[ \left( \frac{Y_\chi}{Y_\chi^{\text{eq}}} \right)^2 - \left( \frac{Y_{N_i}}{Y_{N_i}^{\text{eq}}} \right)^2 \right] 2\gamma_{\chi\chi \rightarrow N_i N_i} \\ & - \frac{z}{sH(m_{N_1})} \left[ \left( \frac{Y_\chi}{Y_\chi^{\text{eq}}} \right)^2 - 1 \right] \left( 2\gamma_{\chi\chi \rightarrow \rho\rho, Z'Z'} + 2\gamma_{\chi\chi \rightarrow \rho Z', hZ'} + 2\gamma_{\chi\chi \rightarrow \text{SM}} \right), \end{aligned} \quad (4.2)$$

$$\begin{aligned} \frac{dY_{B-L}}{dz} = & \sum_{i=1,2} \frac{z}{sH(m_{N_1})} \left[ \varepsilon_i \left( \frac{Y_{N_i}}{Y_{N_i}^{\text{eq}}} - 1 \right) - \frac{Y_{B-L}}{2Y_\ell^{\text{eq}}} \right] \gamma_{N_i \rightarrow \ell H} \\ & - \sum_{i=1,2} \frac{z}{sH(m_{N_1})} \frac{Y_{B-L}}{Y_\ell^{\text{eq}}} \left( \frac{Y_{N_i}}{Y_{N_i}^{\text{eq}}} \gamma_{N_i \ell \rightarrow qt} + 2\gamma_{N_i t \rightarrow ql} \right). \end{aligned} \quad (4.3)$$

The physical quantities appearing in the above system are defined as follows:

- $Y_X \equiv n_X/s$ : comoving number density of the species  $X$ ;
- $Y_X^{\text{eq}}$ : equilibrium comoving number density;
- $H(m_{N_1})$ : Hubble expansion rate evaluated at  $T = m_{N_1}$ ;
- $\varepsilon_i$ : CP asymmetry generated in the decay of  $N_i$  [47, 57, 88–90];
- $\gamma_{a \rightarrow b}$ ,  $\gamma_{ab \rightarrow cd}$ : thermally averaged reaction densities for decay and scattering processes [47, 81].

Explicit expressions for the thermally averaged  $\gamma$  functions can be found in Refs. [81, 83].

At early times, all species are assumed to be in thermal equilibrium with the plasma, such that  $Y_X = Y_X^{\text{eq}}$  for each particle species  $X$ . As the Universe expands and cools, the interaction rates of  $N_i$  and  $\chi$  eventually fall below the Hubble expansion rate, making these species decouple from the thermal bath. The freeze-out of  $\chi$  determines its present relic

density [67, 97], while the departure of  $N_i$  from equilibrium combined with CP-violating decays produces a net lepton asymmetry. Subsequently, this asymmetry is converted into the observed BAU through electroweak sphaleron transitions [50–52, 96], thereby establishing a unified thermal origin for both DM and baryogenesis within the model [74, 76, 99].

## 5 Numerical Analysis

To explore the phenomenological viability of our framework, we perform a comprehensive numerical study that covers both the DM and leptogenesis sectors. The model is characterized by the following set of independent parameters:

$$\{m_\rho, m_{Z'}, M_{N_1}, M_{N_2}, m_\chi, m_{\nu_0}, v_\phi, \theta, y_\nu\}. \quad (5.1)$$

These parameters denote the masses of the additional scalar  $\rho$ , the  $U(1)_{B-L}$  gauge boson  $Z'$ , the two heavy Majorana neutrinos  $N_{1,2}$ , and the DM fermion  $\chi$ , as well as the light neutrino mass scale  $m_{\nu_0}$ , the VEV of the scalar field  $\phi$ , the scalar mixing angle  $\theta$ , and the Yukawa coupling matrix  $y_\nu$ , respectively.

We perform a detailed parameter scan to identify the parameter regions consistent with current cosmological and experimental observations. The analysis focuses on reproducing the measured DM relic density, generating the correct baryon asymmetry through low-scale leptogenesis, and satisfying the latest direct-detection bounds from the LZ-2024 experiment [98]. The cosmological observables used as input constraints are

$$Y_B^{\text{obs}} \simeq 8.7 \times 10^{-11}, \quad \Omega_{\text{DM}} h^2 \simeq 0.12, \quad (5.2)$$

which correspond to the observed baryon-to-entropy ratio and the DM relic abundance, respectively.

For each point in the scan, we also impose requirements from neutrino oscillation data [78] and LFV processes [79, 80]. The light-neutrino mass matrix is constructed from the chosen heavy-neutrino spectrum and Yukawa couplings, and only those points that reproduce the observed mass-squared differences and mixing angles are kept. For the same parameter set, we solve the Boltzmann equations discussed in the previous section and compute the resulting baryon asymmetry yield  $Y_B$ . The loop-induced amplitudes for the radiative LFV transitions  $\ell_i \rightarrow \ell_j \gamma$  are evaluated to ensure compatibility with the corresponding experimental upper limits. Only points satisfying *all* of these conditions are regarded fully viable.

To remain compatible with collider searches for heavy dilepton resonances [100, 101], we fix the  $Z'$  mass to  $m_{Z'} = 7$  TeV, which lies safely above the current experimental lower limit of  $m_{Z'} \gtrsim 5.15$  TeV. Furthermore, to respect the spin-independent scattering bounds from LZ-2024 [98], the scalar mixing angle is chosen to be small,  $\theta \sim \mathcal{O}(0.01)$ , ensuring that the Higgs-portal contribution to direct detection remains well below the current experimental sensitivity while retaining efficient annihilation through the gauge interaction.

The outcome of the full parameter scan in the leptogenesis sector is illustrated in Figs. 3 and 4. First, Fig. 3 shows the parameter dependence of the CP asymmetry  $\varepsilon_1$

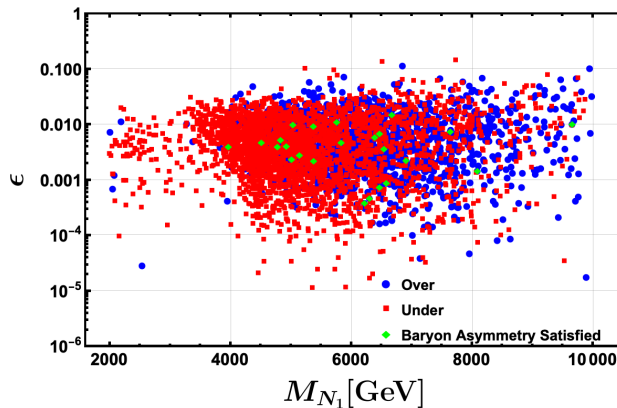


**Figure 3.** Parameter scan in the  $(M_{N_1}, \epsilon)$  plane showing the regions corresponding to over-abundant (blue) and under-abundant (red) DM relic density. The green points satisfy the observed BAU. Here  $M_{N_1}$  denotes the mass of the lightest heavy neutrino, while  $\epsilon$  represents the CP-asymmetry parameter relevant for leptogenesis.

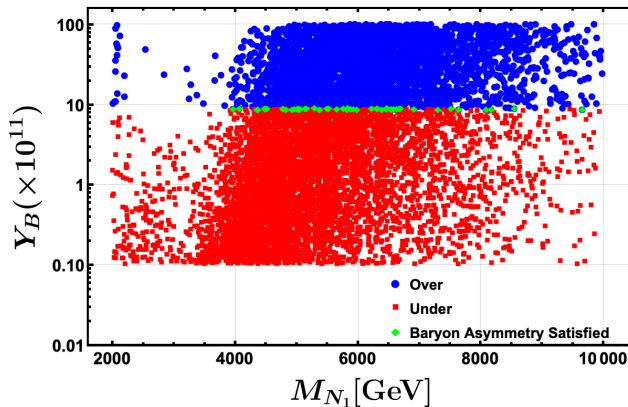


**Figure 4.** Baryon asymmetry yield  $Y_B$  as a function of the lightest heavy-neutrino mass  $M_{N_1}$ . The blue points correspond to parameter regions leading to over-abundant DM relic density, while the red points denote under-abundant relic-density regions. The green points satisfy the observed BAU and all constraints from DM, neutrino oscillations, direct detection, and LFV processes.

generated in the decay of  $N_1$ . A narrow resonant band appears when  $M_{N_1}$  and  $M_{N_2}$  are quasi-degenerate, where  $\epsilon_1$  is significantly enhanced, in agreement with the expectations of resonant leptogenesis. Away from this quasi-degenerate region, the CP asymmetry rapidly decreases, and successful leptogenesis becomes impossible.

The resulting baryon asymmetry yield  $Y_B$  obtained from solving the full Boltzmann equations for each scanned point is presented in Fig. 4. The green points in this plot denote the subset of points that *simultaneously* reproduce the observed baryon asymmetry and satisfy all phenomenological constraints, namely the DM relic density, neutrino oscillation data, direct-detection limits, and the LFV bounds on  $\ell_i \rightarrow \ell_j \gamma$ . These green points are therefore identified as the fully allowed region of the model.

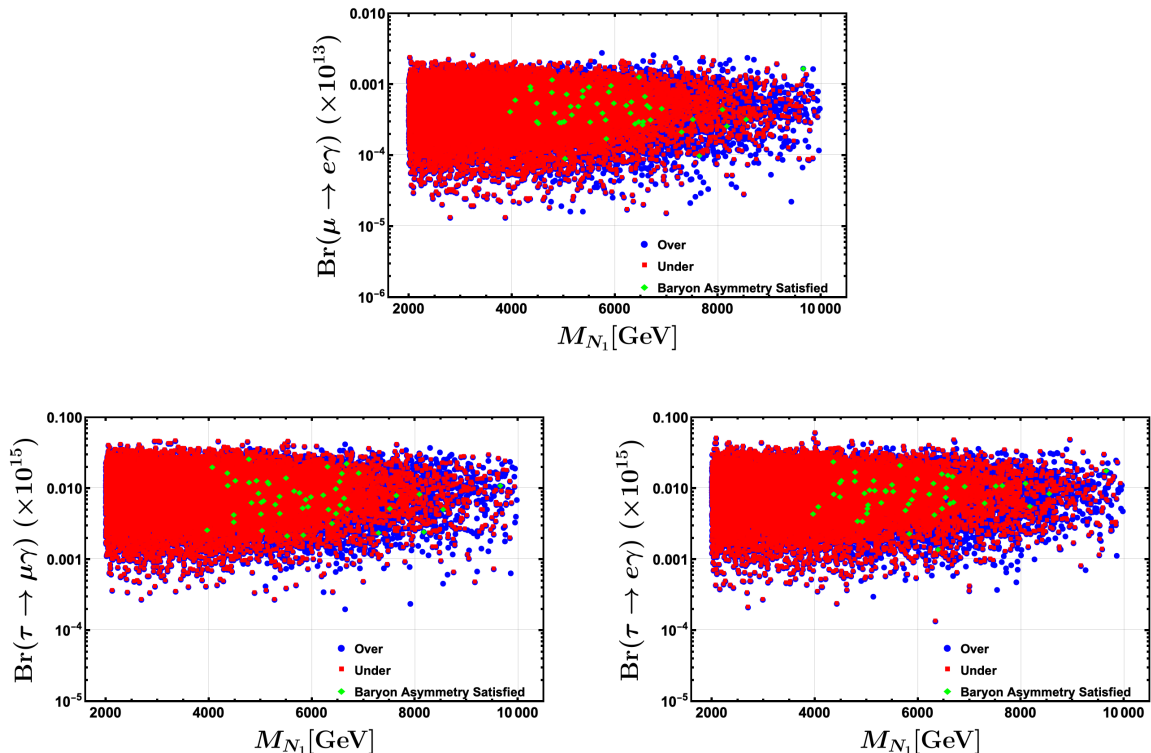


**Figure 5.** Predicted branching ratios of the radiative LFV processes as functions of the lightest heavy neutrino mass  $M_{N_1}$ . The blue and red points correspond to parameter regions yielding over-abundant and under-abundant DM relic density respectively, while the green points satisfy the observed BAU.

The complementary impact of the LFV constraints is shown in Fig. 5, which displays the predicted branching ratios for the radiative LFV decays  $\ell_i \rightarrow \ell_j \gamma$  within the same parameter space. Each point corresponds to a fully numerical evaluation of the loop-induced amplitude for the chosen set of masses and Yukawa couplings. The plots demonstrate that the green points in Fig. 4 lie comfortably below the current experimental upper limits on these LFV processes, while the regions outside tend to generate larger LFV rates and are more strongly constrained.

From the allowed green points, we select two representative benchmark points, which satisfy all the phenomenological constraints discussed above: reproducing the observed neutrino oscillation pattern, achieving the correct DM relic abundance through  $Z'$ -mediated annihilation, generating the observed baryon asymmetry through resonant leptogenesis, and respecting the bounds from  $\ell_i \rightarrow \ell_j \gamma$ . In both cases, the mass of the lightest heavy neutrino satisfies

$$M_{N_1} \sim \mathcal{O}(1\text{--}10 \text{ TeV}), \quad (5.3)$$

which keeps the scenario experimentally testable, since such states can be produced at future high-energy colliders, in particular at multi-TeV muon colliders.

In summary, the interplay between the  $Z'$ -mediated annihilation of DM, the suppressed

**Table 1.** Benchmark parameter sets consistent with the observed DM relic abundance, baryon asymmetry, and recent LZ-2024 direct detection limits. The relation  $m_\chi \simeq 2m_{N_1}$  and small scalar mixing  $\theta \sim \mathcal{O}(0.01)$  are crucial for ensuring compatibility with all the current experimental and cosmological observations.

Parameter	Benchmark 1 (BP1)	Benchmark 2 (BP2)
$m_{Z'}$ [GeV]	7000	7000
$m_\rho \equiv M_{H_2}$ [GeV]	500	500
$m_\chi$ [GeV]	8200	8737
$M_{N_1}$ [GeV]	4100	4368
$M_{N_2}$ [GeV]	4100	4368
$v_\phi$ [GeV]	5000	5000
$\theta$	$\mathcal{O}(0.01)$	$\mathcal{O}(0.01)$

scalar mixing, the quasi-degenerate heavy-neutrino spectrum, and the LFV constraints yields a narrow yet phenomenologically viable region of parameter space. Within this domain, both the DM relic density and the observed baryon asymmetry can be simultaneously reproduced without conflicting with collider, direct-detection, or flavor data. Representative benchmark points that satisfy all the experimental and cosmological requirements are listed in Table 1.

## 6 Collider Phenomenology

The parameter space selected in the preceding section, where the DM relic abundance, the direct- and indirect-detection limits, and the  $B-L$  asymmetry are simultaneously satisfied, naturally points to a TeV-scale spectrum for the new states.

At hadron colliders, the Drell-Yan production of  $Z'$  followed by  $Z' \rightarrow \ell^+ \ell^-$  provides the leading probe of the gauge sector. Present dilepton searches push  $m_{Z'}$  to several TeV, which is well accommodated in the chosen benchmarks. Direct production of the heavy neutrinos at the LHC suffers from small cross sections and substantial SM backgrounds, making discovery challenging with cut-based selections. A lepton collider with centre-of-mass energies in the few to 10 TeV range and clean experimental conditions offers substantially improved sensitivity to TeV-scale heavy neutrinos through active-sterile mixing. A future muon collider, in particular, would be ideally suited to realise this potential.

At a muon collider, the dominant production mechanism for heavy Majorana neutrinos is the single-production process

$$\mu^+ \mu^- \rightarrow N_i \nu_\ell \quad (\ell = e, \mu, \tau), \quad (6.1)$$

mediated primarily by the  $t$ -channel  $W$  exchange, with the sub-leading  $s$ -channel  $Z$  contributions controlled by the active-sterile mixing. The produced heavy neutrino subsequently

decays via

$$N_i \rightarrow W^\pm \ell^\mp, \quad N_i \rightarrow Z \nu_\ell, \quad N_i \rightarrow h \nu_\ell, \quad (6.2)$$

leading to two characteristic final-state signatures: a fully leptonic dilepton mode,  $2\ell + \cancel{E}_T$ , arising from  $W^\pm \rightarrow \ell^\pm \nu_\ell$ , and a semi-leptonic mode,  $1\ell + 2j + \cancel{E}_T$ , resulting from the hadronic decay  $W^\pm \rightarrow jj$ . These two channels provide complementary sensitivity to the heavy-neutrino dynamics.

Before discussing these channels, we make an important comment. A major experimental challenge at high-energy muon colliders is the presence of a beam-induced background (BIB), originating from the decay of muons in the circulating beams [102–104]. These decays generate a large flux of predominantly soft, low-energy particles that can significantly affect detector performance if not properly mitigated. Dedicated mitigation strategies, such as shielding nozzles in the forward region and high-precision timing in tracking and calorimeter systems, have been shown to substantially suppress this background. For the signal processes considered in this work, involving heavy neutrinos with masses of order  $\mathcal{O}(4 \text{ TeV})$ , the resulting final states are characterized by highly energetic charged leptons and, in the semi-leptonic channel, hard jets. The transverse momenta of these objects are significantly larger than the typical energy scale associated with BIB particles. Imposing a selection requirement of  $p_T > 10 \text{ GeV}$  for charged leptons within the detector acceptance  $|\eta| < 2.5$  efficiently suppresses the dominant BIB contributions. Therefore, for the benchmark scenarios considered in this analysis, the BIB impact is expected to be subdominant and does not significantly affect the signal sensitivity.

### 6.1 Dilepton Final State $2\ell + \cancel{E}_T$

A particularly clean final state arises when the heavy neutrino decays through

$$N_i \rightarrow W^\pm \ell^\mp, \quad W^\pm \rightarrow \ell^\pm \nu_\ell, \quad (6.3)$$

leading to the process

$$\mu^+ \mu^- \rightarrow N_i \nu_\ell \rightarrow (\ell W) \nu_\ell \rightarrow \ell^+ \ell^- + \cancel{E}_T. \quad (6.4)$$

The dominant SM backgrounds include  $\mu^+ \mu^- \rightarrow W^+ W^- \rightarrow \ell^+ \ell^- + \cancel{E}_T$ , off-shell  $Z/\gamma^* \rightarrow \ell^+ \ell^-$  in association with neutrinos, and multi-boson processes with leptonic decays. The analysis strategy is therefore based on basic acceptance cuts, hardness requirements on the lepton transverse momenta, a veto around the  $Z$  pole in  $m_{\ell\ell}$  to suppress  $Z$ -mediated backgrounds, and cuts on  $\cancel{E}_T$  and angular variables (such as  $\Delta\phi(\ell\ell)$ ) to reduce  $WW$ - and  $ZZ$ -induced contributions.

The signal and background samples are produced at leading order (LO) with the aid of MG5aMC@NLO [105]. Parton showering and hadronization are performed with Pythia8 [106, 107], and the detector response is modeled using Delphes [108], with a configuration appropriate for the proposed muon-collider. The jets are reconstructed with a collider-appropriate algorithm (e.g. the Valencia (VLC) [109, 110] algorithm) with radius  $R = 0.5$ .

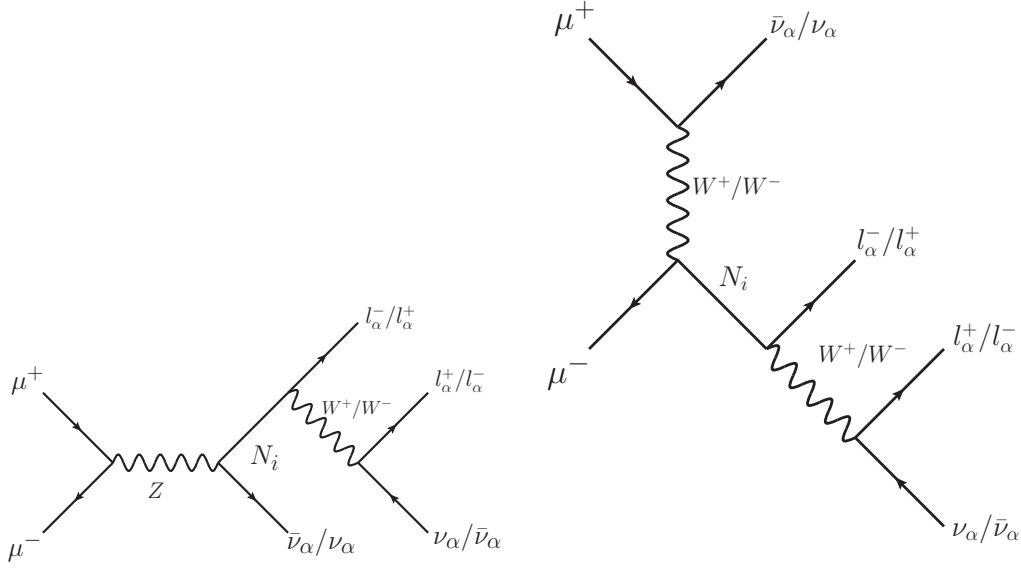


**Figure 6.** Representative Feynman diagrams for single heavy-neutrino production at a muon collider,  $\mu^+\mu^- \rightarrow N_i\nu_\ell$ , followed by  $N_i \rightarrow W^\pm\ell^\mp$  and  $W^\pm \rightarrow \ell^\pm\nu_\ell$ , leading to the  $\ell^+\ell^- + \cancel{E}_T$  final state.

Unless stated otherwise, the nominal object selections adopt

$$\begin{aligned}
p_{Tj} &> 20 \text{ GeV}, & |\eta_j| &< 5.0, \\
p_{T\ell} &> 10 \text{ GeV}, & |\eta_\ell| &< 2.5, \\
\Delta R_{ij} &> 0.4, & i, j &= \{\ell, \text{jet}\},
\end{aligned} \tag{6.5}$$

with  $\Delta R_{ij} = \sqrt{(\eta_i - \eta_j)^2 + (\phi_i - \phi_j)^2}$ .

We focus on a final state characterized by two opposite-sign leptons, having the same or different flavor, and missing transverse energy,  $\ell^+\ell^- + \cancel{E}_T$ , originating from

$$\mu^+\mu^- \rightarrow N\nu_\ell, \quad N \rightarrow W^\pm\ell^\mp, \quad W^\pm \rightarrow \ell^\pm\nu_\ell(\bar{\nu}_\ell), \tag{6.6}$$

where the heavy neutrino decays to a  $W^\pm$  and a charged lepton through charged-current interactions, followed by the leptonic decay of  $W^\pm$ . Representative Feynman diagrams for the signal process are shown in Fig. 6. The primary SM background mimicking this final state is  $\mu^+\mu^- \rightarrow \ell^+\ell^- + \cancel{E}_T$ , with dominant contributions from the following sub-processes:

- $\mu^+\mu^- \rightarrow \ell^-\ell^+ \rightarrow \ell^-W^{+\ast}\bar{\nu}_\ell \rightarrow \ell^-\ell^+\nu_\ell\bar{\nu}_\ell$ ,
- $\mu^+\mu^- \rightarrow \ell^-\ell^+ \rightarrow \ell^-Z^\ast\ell^+ \rightarrow \ell^-\ell^+\nu_\ell\bar{\nu}_\ell$ ,
- $\mu^+\mu^- \rightarrow \nu_i^\ast\nu_\ell \rightarrow \nu_\ell Z^\ast\bar{\nu}_\ell \rightarrow \nu_\ell\bar{\nu}_\ell\ell^+\ell^-$ ,
- $\mu^+\mu^- \rightarrow \nu_i^\ast\bar{\nu}_\ell \rightarrow \bar{\nu}_\ell W^\ast\ell^- \rightarrow \nu_\ell\bar{\nu}_\ell\ell^+\ell^-$ ,
- $\mu^+\mu^- \rightarrow W^+W^-, ZZ, W^+W^-Z, ZZZ$  with leptonic and semi-leptonic decays.

**Table 2.** LO cross sections for the process  $\mu^+\mu^- \rightarrow 2\ell + \cancel{E}_T$  at  $\sqrt{s} = 6$  and 10 TeV for the signal benchmarks and the SM background.

Benchmark	$\sigma_{\text{LO}}$ (fb) @ $\sqrt{s} = 6$ TeV	$\sigma_{\text{LO}}$ (fb) @ $\sqrt{s} = 10$ TeV
BP1 Signal	25	373
BP2 Signal	20	285
Background	233	198

The LO cross sections for the process  $\mu^+\mu^- \rightarrow 2\ell + \cancel{E}_T$  at  $\sqrt{s} = 6$  and 10 TeV for the signal benchmarks and the total SM background are given in Table 2.

To design an efficient set of analysis cuts, we first examine the shapes of several kinematic observables for the signal and the SM background. From this exercise, three distributions are found to provide the most effective discrimination between signal and background: the transverse momenta of the leading and sub-leading leptons,  $p_T^{\ell_1}$  and  $p_T^{\ell_2}$ , and the missing transverse energy  $\cancel{E}_T$ . Figs. 7 and 8 show the corresponding normalized distributions for the two signal benchmarks (BP1 and BP2) and the SM background at  $\sqrt{s} = 6$  and 10 TeV, respectively. All distributions are normalized to unity to emphasize shape differences rather than absolute event rates.

From Figs. 7 and 8, we can see that the  $p_T^{\ell_1}$  distribution (top-left panel) of the leading lepton in the signal is typically much harder than in the SM background, reflecting the large mass scale of the heavy neutrino produced. A similar, though somewhat milder, behavior is observed for  $p_T^{\ell_2}$  (top-right panel), where the sub-leading lepton originating from the  $W$  decay remains significantly harder in the signal than in the background. The missing transverse energy distribution (bottom panel) also exhibits a characteristic separation between signal and background, thereby providing an additional handle to suppress background events while retaining most of the signal. The same qualitative features observed at both center-of-mass energies motivate the use of an identical set of kinematic selection criteria in the subsequent analysis.

Guided by these kinematic distributions, we define the following sequence of selection cuts, denoted by  $B_i$  for the  $\sqrt{s} = 6$  TeV analysis:

- **$B_1$  (dilepton preselection):** we require exactly two isolated, oppositely charged leptons (electrons or muons) in the final state, and satisfying the basic acceptance criteria

$$p_{T^\ell} > 10 \text{ GeV}, \quad |\eta_\ell| < 2.5, \quad \Delta R_{\ell\ell} > 0.4.$$

- **$B_2$  (hard leading lepton):** taking advantage of the harder  $p_T^{\ell_1}$  spectrum of the signal compared to the background (top-left panel of Fig. 7), we impose

$$p_T^{\ell_1} > 250 \text{ GeV},$$

which removes a large fraction of the SM background while leaving the bulk of the signal events unaffected.

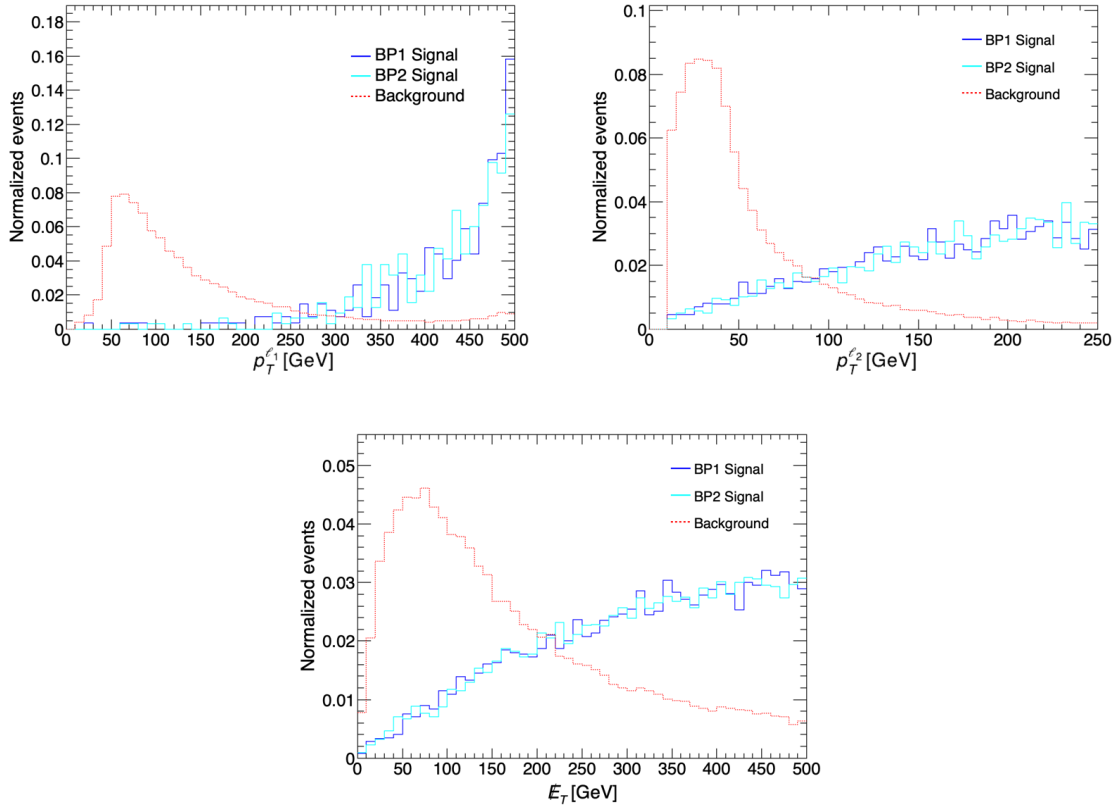


**Figure 7.** Normalized distributions of key kinematic observables for the process  $\mu^+\mu^- \rightarrow 2\ell + \cancel{E}_T$  at  $\sqrt{s} = 6$  TeV: leading lepton transverse momentum  $p_T^{\ell_1}$  (top-left), sub-leading lepton transverse momentum  $p_T^{\ell_2}$  (top-right), and missing transverse energy  $\cancel{E}_T$  (bottom). The curves correspond to the two signal benchmarks (BP1 and BP2) and the total SM background. These distributions are used to construct the optimized kinematic selections.

- **$B_3$  (hard sub-leading lepton):** as can be seen from the top-right panel of Fig. 7, the sub-leading lepton is also significantly harder in the signal. We therefore demand

$$p_T^{\ell_2} > 100 \text{ GeV},$$

efficiently suppressing the background configurations in which the second lepton is soft.

- **$B_4$  (missing-energy selection):** guided by the shapes in the bottom panel of Fig. 7, we apply a cut on the missing transverse energy,

$$\cancel{E}_T < 250 \text{ GeV},$$

which retains most of the signal while eliminating a substantial portion of the high- $\cancel{E}_T$  background tail.

The impact of these selections on the signal and background event yields is summarized in the cut-flow presented in Table 3. After applying the complete set of cuts  $B_1$ – $B_4$ , both the

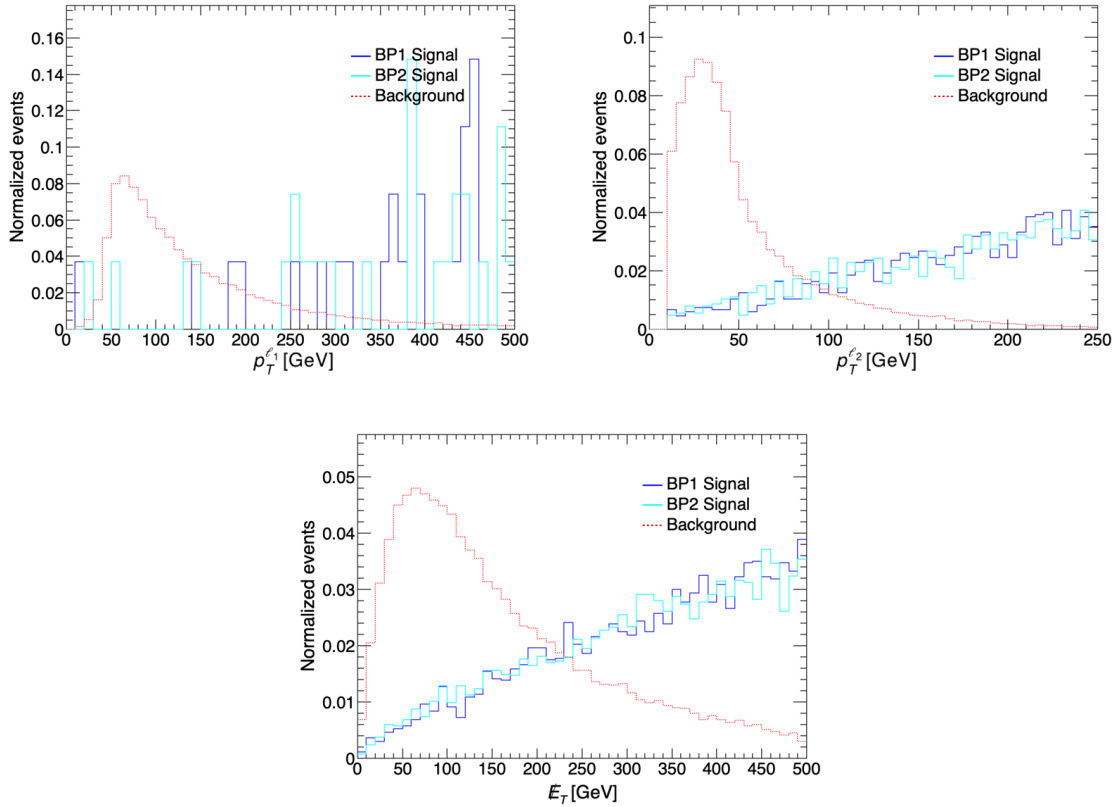


**Figure 8.** Same as in Fig. 7 but at  $\sqrt{s} = 10$  TeV.

signal-to-background ratio and the statistical significance are significantly enhanced. For the benchmark scenarios considered, the integrated luminosity required to reach the  $5\sigma$  discovery threshold in the  $\ell^+\ell^- + \cancel{E}_T$  channel is at the level of a few  $\text{fb}^{-1}$  at  $\sqrt{s} = 6$  TeV, and is further reduced at  $\sqrt{s} = 10$  TeV due to the increased signal production rate.

## 6.2 $1\ell + 2j + \cancel{E}_T$ Final State

A complementary and often more sensitive channel at a high-energy muon collider is the single-lepton plus dijet final state accompanied by missing transverse energy. In this topology, the heavy neutrino is produced in association with an active neutrino and subsequently undergoes a charged-current decay,

$$\mu^+\mu^- \rightarrow \nu_\ell N_i, \quad N_i \rightarrow W^\pm \ell^\mp, \quad W^\pm \rightarrow jj, \quad (6.7)$$

leading to the final state  $\ell^\pm + 2j + \cancel{E}_T$ . Representative Feynman diagrams for the signal process are shown in Fig. 9. Compared to the fully leptonic mode, this channel benefits from the larger hadronic branching fraction of the  $W$  boson and typically offers higher event rates.

The final-state particles are clustered into exactly two jets using a radius parameter of  $R = 0.5$ , ensuring stable reconstruction for multi-TeV kinematics. The jets are reconstructed using the VLC algorithm [109, 110], which is well suited for the clean environment

**Table 3.** Cut-flow for signal and background events after sequential cuts  $B_1$ – $B_4$  at  $\sqrt{s} = 6$  and 10 TeV, together with the integrated luminosity  $\mathcal{L}_{5\sigma}$  required to reach  $5\sigma$  significance.

Benchmark	$B_1$	$B_2$	$B_3$	$B_4$	$\mathcal{L}_{5\sigma}$ (fb $^{-1}$ )
$\sqrt{s} = 6$ TeV					
SM Background	19033	8695	4862	3870	–
BP1 Signal	1967	1966	1775	1263	4.5
BP2 Signal	1570	1569	1543	1003	5.7
$\sqrt{s} = 10$ TeV					
SM Background	15858	5166	2796	2796	–
BP1 Signal	29017	29016	28853	28853	0.095
BP2 Signal	22113	22112	21982	21982	0.128

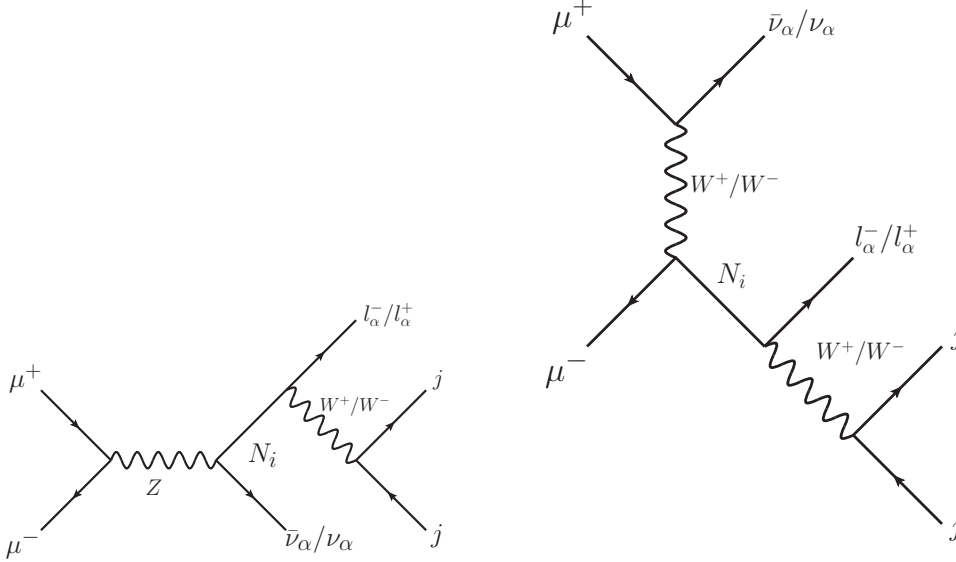


**Figure 9.** Representative Feynman diagrams for single heavy-neutrino production at a muon collider,  $\mu^+\mu^- \rightarrow N_i\nu_\ell$ , followed by  $N_i \rightarrow W^\pm\ell^\mp$  and  $W^\pm \rightarrow jj$ , leading to the  $\ell^\pm + 2j + \cancel{E}_T$  final state.

and boosted topologies at lepton colliders. The main SM processes capable of mimicking this signature are

- $\mu^+\mu^- \rightarrow W^+W^- \rightarrow \ell^\pm\nu_\ell jj$ ,
- $\mu^+\mu^- \rightarrow ZZ$  with  $Z \rightarrow jj$  and one lepton missed,
- $\mu^+\mu^- \rightarrow W^+W^-Z$  with partially leptonic  $W$  decays,
- $\mu^+\mu^- \rightarrow ZZZ$  with  $Z \rightarrow jj$  and invisible decays,

**Table 4.** LO cross sections for the process  $\mu^+\mu^- \rightarrow 1\ell + 2j + \cancel{E}_T$  at  $\sqrt{s} = 6$  and 10 TeV.

Benchmark	$\sigma_{\text{LO}}$ (fb) at $\sqrt{s} = 6$ TeV	$\sigma_{\text{LO}}$ (fb) at $\sqrt{s} = 10$ TeV
BP1 Signal	77	1117
BP2 Signal	67	855
$W^+W^-$	62.55	25.69
$W^+W^-Z$	11.04	9.44
$ZZ$	$3.65 \times 10^{-2}$	$1.49 \times 10^{-2}$
$Zh$	0.34	0.123
$ZZZ$	$4.93 \times 10^{-5}$	$2.573 \times 10^{-5}$

- $\mu^+\mu^- \rightarrow Zh$  with  $h \rightarrow jj$  and a missed lepton.

After basic acceptance cuts, the  $W^+W^-$  and  $W^+W^-Z$  processes constitute the dominant irreducible backgrounds.

Table 4 summarizes the LO cross sections for the signal benchmarks and the dominant SM backgrounds for the  $1\ell + 2j + \cancel{E}_T$  final state at  $\sqrt{s} = 6$  and 10 TeV. At  $\sqrt{s} = 6$  TeV, the signal rates are already sizable, with  $\sigma_{\text{BP1}} = 77$  fb and  $\sigma_{\text{BP2}} = 67$  fb. These values originate from the enhanced single-production channel  $\mu^+\mu^- \rightarrow N\nu_\ell$  mediated by  $t$ -channel  $W$  exchange, which becomes increasingly efficient at multi-TeV center-of-mass energies and enables the probing of TeV-scale heavy neutrinos with appreciable production rates. Among the SM backgrounds, the  $W^+W^-$  process constitutes the dominant contribution, with a cross section of 62.55 fb in the semi-leptonic topology relevant for the  $1\ell + 2j + \cancel{E}_T$  final state. The next most significant background arises from the  $W^+W^-Z$  production, yielding 11.04 fb once the decay modes with  $Z \rightarrow jj$  and  $Z \rightarrow \nu\bar{\nu}$  are included. Other electroweak channels, such as  $ZZ$ ,  $Zh$ , and  $ZZZ$ , are strongly suppressed, contributing at the sub-femtobarn or even  $10^{-2}$  fb level, due to smaller electroweak couplings and the reduced phase space for multi-boson final states at  $\sqrt{s} = 6$  TeV.

At  $\sqrt{s} = 10$  TeV, the signal cross sections increase by more than an order of magnitude, while the dominant backgrounds exhibit a much weaker energy dependence. As a result, the signal-to-background hierarchy before selection cuts becomes even more favorable at higher energies. In general, the heavy-neutrino signal lies well above most SM backgrounds at the inclusive level and is primarily challenged by the  $W^+W^-$  and  $W^+W^-Z$  channels.

To construct an efficient set of selection criteria, we examine the shapes of key observables sensitive to the presence of a heavy neutrino. Figures 10 and 11 show the normalized distributions of the transverse momenta of the leading and sub-leading jets,  $p_T^{j_1}$  and  $p_T^{j_2}$ , for the signal benchmarks and the dominant backgrounds at  $\sqrt{s} = 6$  and 10 TeV. In both cases, the signal distributions are characterized by substantially harder jet spectra than those of the background, reflecting the boosted hadronic  $W$  boson produced in the decay of a multi-TeV heavy neutrino. The separation between signal and background is striking,

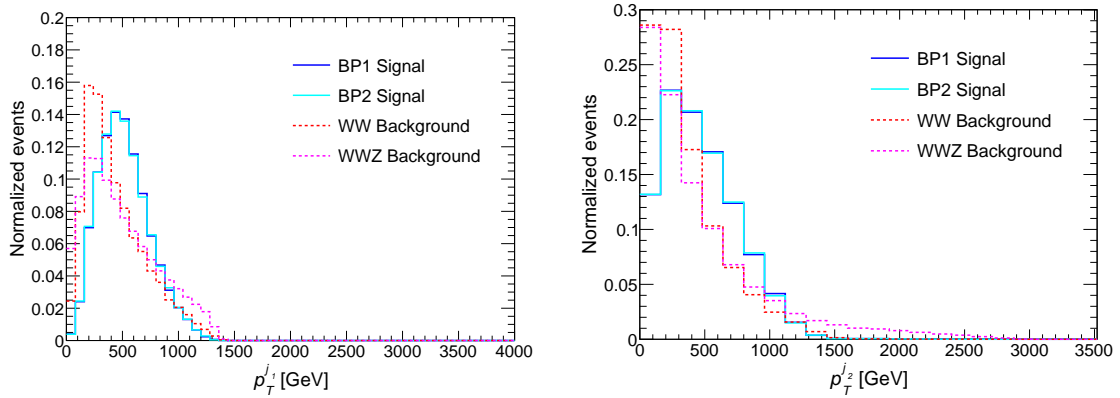


**Figure 10.** Normalized transverse momentum distributions of the jets for the  $1\ell + 2j + \cancel{E}_T$  final state at  $\sqrt{s} = 6$  TeV. Left: leading jet  $p_T^{j_1}$ . Right: sub-leading jet  $p_T^{j_2}$ . Signal benchmarks BP1 and BP2 exhibit significantly harder jet spectra than the  $W^+W^-$  and  $W^+W^-Z$  backgrounds, reflecting the multi-TeV mass of the parent heavy neutrino. These features motivate the high- $p_T$  selections adopted in the analysis.

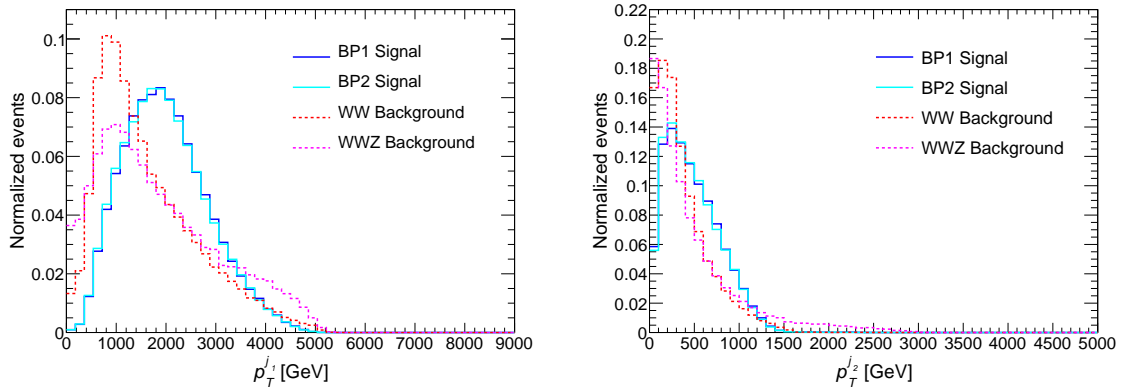


**Figure 11.** Same as in Fig. 10 but at  $\sqrt{s} = 10$  TeV.

based on the following observations:

- The leading jet from  $W \rightarrow jj$  in heavy neutrino decays carries a large fraction of the heavy neutrino mass, producing a peak well above 1–2 TeV for the two benchmarks.
- The sub-leading jet is also harder than that of the background, typically exceeding several hundred GeV.
- The background jets from  $W^+W^-$  peak at significantly lower  $p_T$ , reflecting the SM  $W$  mass scale.

These observations make the  $1\ell + 2j + \cancel{E}_T$  channel a powerful discriminator by applying high- $p_T$  jet selections.

Motivated by the distributions shown in Figs. 10 and 11, we adopt the following optimized requirements:

**Table 5.** Cut-flow for the  $1\ell + 2j + \cancel{E}_T$  final state at  $\sqrt{s} = 6$  and 10 TeV, showing event yields after applying the leading-jet ( $p_T^{j_1} > 800$  GeV) and sub-leading-jet ( $p_T^{j_2} > 400$  GeV) selections. The integrated luminosity  $\mathcal{L}_{5\sigma}$  required to reach  $5\sigma$  significance is also shown.

<b>Benchmark</b>	Before cut	$J_1$	$J_2$	$\mathcal{L}_{5\sigma}$ (fb $^{-1}$ )
$\sqrt{s} = 6$ TeV				
$W^+W^-$	6255	424	209	–
$W^+W^-Z$	1104	210	127	–
BP1 Signal	7700	4735	2827	0.88
BP2 Signal	6100	3741	2229	1.02
$\sqrt{s} = 10$ TeV				
$W^+W^-$	2565	295	233	–
$W^+W^-Z$	944	140	110	–
BP1 Signal	111700	91704	86101	0.029
BP2 Signal	85500	70210	65802	0.038

- **Cut J1 (leading jet):**

$$p_T^{j_1} > 800 \text{ GeV.}$$

- **Cut J2 (sub-leading jet):**

$$p_T^{j_2} > 400 \text{ GeV.}$$

The numerical values shown in Table 5 quantify the impact of the jet-based selections on the heavy-neutrino signal and the dominant electroweak backgrounds. All event yields are shown for a common reference with an integrated luminosity of 100 fb $^{-1}$ . At  $\sqrt{s} = 6$  TeV, the dominant background contributions arise from the  $W^+W^-$  and  $W^+W^-Z$  productions, yielding 6255 and 1104 events respectively, before the application of any analysis cuts. The corresponding signal yields for the benchmark points BP1 and BP2 are 7700 and 6100 events, indicating that the signal already competes with the leading backgrounds at the inclusive level.

Imposing the leading-jet requirement  $p_T^{j_1} > 800$  GeV (cut  $J_1$ ) results in a strong suppression of the backgrounds at  $\sqrt{s} = 6$  TeV: the  $W^+W^-$  yield is reduced from 6255 to 424 events, and the  $W^+W^-Z$  contribution from 1104 to 210 events. In contrast, the signal retains a large fraction of events, with BP1 decreasing from 7700 to 4735 and BP2 from 6100 to 3741 events. This behavior directly reflects the characteristic hardness of the jets in the signal, which is largely absent in SM diboson production.

The additional requirement on the sub-leading jet,  $p_T^{j_2} > 400$  GeV (cut  $J_2$ ), further sharpens the discrimination. After this selection, the  $W^+W^-$  background is reduced to 209 events, while the  $W^+W^-Z$  background decreases to 127 events. The signal remains comparatively robust, with 2827 events for BP1 and 2229 events for BP2. In general,

the combined jet selections suppress the dominant backgrounds by factors of  $\mathcal{O}(30)$ , while preserving approximately one third of the signal, in line with expectations for a boosted two-jet system arising from heavy-neutrino decay.

At  $\sqrt{s} = 10$  TeV, the inclusive signal yields increase dramatically, reaching 111700 events for BP1 and 85500 events for BP2 before cuts, while the dominant backgrounds remain at the level of a few thousand events. As a result, the signal-to-background ratio is already highly favorable before any kinematic selection. The jet-based requirements are therefore not essential for discovery at this energy, but are instead introduced to enhance sample purity and improve the robustness of the analysis against detector effects and additional reducible backgrounds.

The integrated luminosity required to reach a  $5\sigma$  discovery significance reflects this behavior. At  $\sqrt{s} = 6$  TeV, the values of  $\mathcal{L}_{5\sigma} \simeq 0.88 \text{ fb}^{-1}$  for BP1 and  $\mathcal{L}_{5\sigma} \simeq 1.02 \text{ fb}^{-1}$  for BP2 are sufficient after the full set of selections. At  $\sqrt{s} = 10$  TeV, the required luminosity drops to the level of  $\mathcal{O}(10^{-2}) \text{ fb}^{-1}$ , even with minimal or no jet-based cuts. These results highlight the excellent sensitivity of the  $1\ell + 2j + \cancel{E}_T$  channel at a multi-TeV muon collider, and demonstrate that heavy-neutrino signals can be isolated with high statistical significance using simple and robust selection criteria.

In summary, because the heavy-neutrino production yields clean leptonic and semi-leptonic signatures, while complementary information on the  $U(1)_{B-L}$  gauge sector can be extracted from precision dilepton measurements, a multi-TeV muon collider provides robust sensitivity to the neutrino-sector benchmarks identified in our cosmological analysis. Together with hadron-collider searches for  $Z'$  bosons and non-collider input such as the relic abundance and direct-detection limits, the collider reach presented here completes a coherent and comprehensive test of the parameter region motivated by the DM relic density and successful leptogenesis.

## 7 Conclusion

We have presented a predictive and experimentally testable framework in which the origin of neutrino masses, the BAU, and the nature of DM emerge from a correlated dynamical structure within a local  $U(1)_{B-L}$  extension of the SM. A key distinguishing feature of this construction, relative to previous  $B-L$  scenarios, is the implementation of an inverse-seesaw mechanism that involves the sterile fermion  $S_1$  and the complex scalar field  $\phi$ . The VEV of  $\phi$  generates the masses of the heavy neutrinos and of the Majorana DM particle  $\chi$  through common Yukawa interactions, while a suppressed LNV parameter arising from a higher-dimensional operator yields naturally light active neutrinos together with TeV-scale heavy states that can be probed at colliders.

As the heavy neutrinos, the DM particle, and the  $Z'$  boson all acquire masses from the same  $U(1)_{B-L}$  breaking sector, the early-Universe cosmology is tightly interconnected. A complete numerical solution of the coupled Boltzmann equations was carried out, tracking the evolution of  $N_{1,2}$ ,  $\chi$ , and the net  $B-L$  charge. In this setup, resonant leptogenesis becomes efficient for quasi-degenerate heavy-neutrino masses at the TeV scale. At the same time, the relic abundance of  $\chi$  is dominantly shaped by annihilation through the  $Z'$  portal,

with the correct DM density obtained with a small scalar-Higgs mixing angle that remains consistent with strong direct-detection limits.

A global parameter-space analysis incorporating neutrino oscillation data, radiative LFV processes, DM direct detection, collider constraints on  $N_{1,2}$  and  $Z'$ , and successful baryogenesis identifies a remarkably narrow but stable region in which all requirements are satisfied simultaneously. In this region, representative benchmarks are found with

$$m_{Z'} \simeq 7 \text{ TeV}, \quad m_\chi \simeq 8\text{--}9 \text{ TeV}, \quad M_{N_{1,2}} = \mathcal{O}(4\text{--}5) \text{ TeV}, \quad v_\phi \simeq 5 \text{ TeV}.$$

The inverse-seesaw structure allows light-neutrino masses to be generated with sizable active-sterile mixing and TeV-scale heavy neutrinos, making the sterile sector potentially testable at colliders. In the present setup, this feature is combined with resonant leptogenesis and the  $U(1)_{B-L}$  portal to obtain a correlated explanation of neutrino masses, the BAU, and the DM.

The collider implications of this scenario are equally distinctive. Although LHC dilepton searches already constrain the  $Z'$  mass above the multi-TeV scale, the heavy neutrinos remain elusive at hadron colliders due to small active-sterile mixing and overwhelming backgrounds. In contrast, the clean environment and high-energy reach of future multi-TeV muon colliders provide a uniquely sensitive probe of this model. A detailed Monte-Carlo analysis was performed for both the fully leptonic  $2\ell + \cancel{E}_T$  channel and the hadronic assisted  $1\ell + 2j + \cancel{E}_T$  final state. By exploiting the hardness of leptons, boosted-jet kinematics, and large missing transverse energy, the dominant SM backgrounds can be reduced by more than an order of magnitude while retaining high signal efficiency. For the benchmarks satisfying all cosmological and low-energy constraints, a discovery at the level of  $5\sigma$  is achievable with luminosities of order  $\mathcal{O}(1) \text{ fb}^{-1}$  at  $\sqrt{s} = 6 \text{ TeV}$  and at  $\mathcal{O}(0.1) \text{ fb}^{-1}$  at  $\sqrt{s} = 10 \text{ TeV}$ .

Taken together, the results highlight a coherent and highly constrained scenario in which the inverse-seesaw origin of neutrino masses, the observed baryon asymmetry, and the DM relic density stem all from a single gauge-extended structure. The preferred region of parameter space is not only cosmologically motivated but also within the reach of next-generation experimental programs. In particular, multi-TeV muon colliders, supported by improved LFV searches and DM experiments, offer a realistic possibility of decisively testing this class of models.

We therefore conclude that TeV-scale  $U(1)_{B-L}$  models with an inverse-seesaw structure can simultaneously address several fundamental open problems while remaining sharply predictive. The convergence of cosmological, astrophysical, and collider observables points toward a compelling direction for future exploration, with upcoming facilities poised to validate or exclude this scenario in a definitive manner.

## Acknowledgments

This work is supported by the National Natural Science Foundation of China under Grant Nos. 12475094, 12135006, and 12575099, as well as the Science and Technology Innovation

Leading Talent Support Program of Henan Province under Grant No. 254000510039. XY is also supported in part by the Startup Research Funding from CCNU.

## References

- [1] ATLAS collaboration, *Observation of a new particle in the search for the Standard Model Higgs boson with the ATLAS detector at the LHC*, *Phys. Lett. B* **716** (2012) 1 [[1207.7214](#)].
- [2] CMS collaboration, *Observation of a New Boson at a Mass of 125 GeV with the CMS Experiment at the LHC*, *Phys. Lett. B* **716** (2012) 30 [[1207.7235](#)].
- [3] P.W. Higgs, *Broken Symmetries and the Masses of Gauge Bosons*, *Phys. Rev. Lett.* **13** (1964) 508.
- [4] F. Englert and R. Brout, *Broken Symmetry and the Mass of Gauge Vector Mesons*, *Phys. Rev. Lett.* **13** (1964) 321.
- [5] G.S. Guralnik, C.R. Hagen and T.W.B. Kibble, *Global Conservation Laws and Massless Particles*, *Phys. Rev. Lett.* **13** (1964) 585.
- [6] P.W. Higgs, *Spontaneous Symmetry Breakdown without Massless Bosons*, *Phys. Rev.* **145** (1966) 1156.
- [7] SUPER-KAMIOKANDE collaboration, *Evidence for oscillation of atmospheric neutrinos*, *Phys. Rev. Lett.* **81** (1998) 1562 [[hep-ex/9807003](#)].
- [8] SNO collaboration, *Direct evidence for neutrino flavor transformation from neutral current interactions in the Sudbury Neutrino Observatory*, *Phys. Rev. Lett.* **89** (2002) 011301 [[nucl-ex/0204008](#)].
- [9] PLANCK collaboration, *Planck 2018 results. VI. Cosmological parameters*, *Astron. Astrophys.* **641** (2020) A6 [[1807.06209](#)].
- [10] P. Minkowski,  *$\mu \rightarrow e\gamma$  at a Rate of One Out of  $10^9$  Muon Decays?*, *Phys. Lett. B* **67** (1977) 421.
- [11] R.N. Mohapatra and G. Senjanovic, *Neutrino Mass and Spontaneous Parity Nonconservation*, *Phys. Rev. Lett.* **44** (1980) 912.
- [12] J. Schechter and J.W.F. Valle, *Neutrino Masses in  $SU(2) \times U(1)$  Theories*, *Phys. Rev. D* **22** (1980) 2227.
- [13] J. Schechter and J.W.F. Valle, *Neutrino Decay and Spontaneous Violation of Lepton Number*, *Phys. Rev. D* **25** (1982) 774.
- [14] R.N. Mohapatra et al., *Theory of Neutrinos: A White Paper*, *Rept. Prog. Phys.* **70** (2007) 1757 [[hep-ph/0510213](#)].
- [15] M. Drewes, *The Phenomenology of Right Handed Neutrinos*, *Int. J. Mod. Phys. E* **22** (2013) 1330019 [[1303.6912](#)].
- [16] R.N. Mohapatra, *Mechanism for Understanding Small Neutrino Mass in Superstring Theories*, *Phys. Rev. Lett.* **56** (1986) 561.
- [17] R.N. Mohapatra and J.W.F. Valle, *Neutrino Mass and Baryon Number Nonconservation in Superstring Models*, *Phys. Rev. D* **34** (1986) 1642.

- [18] J. Bernabeu, A. Santamaria, J. Vidal, A. Mendez and J.W.F. Valle, *Lepton Flavor Nonconservation at High-Energies in a Superstring Inspired Standard Model*, *Phys. Lett. B* **187** (1987) 303.
- [19] M.B. Gavela, T. Hambye, D. Hernandez and P. Hernandez, *Minimal Flavour Seesaw Models*, *JHEP* **09** (2009) 038 [[0906.1461](#)].
- [20] M.K. Parida and A. Raychaudhuri, *Inverse see-saw, leptogenesis, observable proton decay and  $\Delta_{\mathbb{R}}^{\pm\pm}$  in SUSY  $SO(10)$  with heavy  $W_{-R}$* , *Phys. Rev. D* **82** (2010) 093017 [[1007.5085](#)].
- [21] J. Garayoa, M.C. Gonzalez-Garcia and N. Rius, *Soft leptogenesis in the inverse seesaw model*, *JHEP* **02** (2007) 021 [[hep-ph/0611311](#)].
- [22] A. Abada and M. Lucente, *Looking for the minimal inverse seesaw realisation*, *Nucl. Phys. B* **885** (2014) 651 [[1401.1507](#)].
- [23] S.S.C. Law and K.L. McDonald, *Generalized inverse seesaw mechanisms*, *Phys. Rev. D* **87** (2013) 113003 [[1303.4887](#)].
- [24] T.P. Nguyen, T.T. Thuc, D.T. Si, T.T. Hong and L.T. Hue, *Low energy phenomena of the lepton sector in an  $A_4$  symmetry model with heavy inverse seesaw neutrinos*, [2011.12181](#).
- [25] T. Asaka and M. Shaposhnikov, *The  $\nu$ MSM, dark matter and baryon asymmetry of the universe*, *Phys. Lett. B* **620** (2005) 17 [[hep-ph/0505013](#)].
- [26] E. Ma, *Common origin of neutrino mass, dark matter, and baryogenesis*, *Mod. Phys. Lett. A* **21** (2006) 1777 [[hep-ph/0605180](#)].
- [27] A. Falkowski, J.T. Ruderman and T. Volansky, *Asymmetric Dark Matter from Leptogenesis*, *JHEP* **05** (2011) 106 [[1101.4936](#)].
- [28] A. Falkowski, E. Kuflik, N. Levi and T. Volansky, *Light Dark Matter from Leptogenesis*, *Phys. Rev. D* **99** (2019) 015022 [[1712.07652](#)].
- [29] T. Hugle, M. Platscher and K. Schmitz, *Low-Scale Leptogenesis in the Scotogenic Neutrino Mass Model*, *Phys. Rev. D* **98** (2018) 023020 [[1804.09660](#)].
- [30] M. Chianese, B. Fu and S.F. King, *Minimal Seesaw extension for Neutrino Mass and Mixing, Leptogenesis and Dark Matter: FIMPzillas through the Right-Handed Neutrino Portal*, *JCAP* **03** (2020) 030 [[1910.12916](#)].
- [31] A. Liu, Z.-L. Han, Y. Jin and F.-X. Yang, *Leptogenesis and dark matter from a low scale seesaw mechanism*, *Phys. Rev. D* **101** (2020) 095005 [[2001.04085](#)].
- [32] M. Fukugita and T. Yanagida, *Baryogenesis Without Grand Unification*, *Phys. Lett. B* **174** (1986) 45.
- [33] L. Covi, E. Roulet and F. Vissani, *CP violating decays in leptogenesis scenarios*, *Phys. Lett. B* **384** (1996) 169 [[hep-ph/9605319](#)].
- [34] E. Roulet, L. Covi and F. Vissani, *On the CP asymmetries in Majorana neutrino decays*, *Phys. Lett. B* **424** (1998) 101 [[hep-ph/9712468](#)].
- [35] A. Pilaftsis, *CP violation and baryogenesis due to heavy Majorana neutrinos*, *Phys. Rev. D* **56** (1997) 5431 [[hep-ph/9707235](#)].
- [36] W. Buchmuller, R.D. Peccei and T. Yanagida, *Leptogenesis as the origin of matter*, *Ann. Rev. Nucl. Part. Sci.* **55** (2005) 311 [[hep-ph/0502169](#)].

- [37] E.J. Chun and K. Turzyski, *Quasi-degenerate neutrinos and leptogenesis from  $L(\mu)$  -  $L(\tau)$* , *Phys. Rev. D* **76** (2007) 053008 [[hep-ph/0703070](#)].
- [38] T. Kitabayashi, *Remark on the minimal seesaw model and leptogenesis with tri/bi-maximal mixing*, *Phys. Rev. D* **76** (2007) 033002 [[hep-ph/0703303](#)].
- [39] C. Martinez-Prieto, D. Delepine and L.A. Urena-Lopez, *Leptogenesis and Reheating in Complex Hybrid Inflation*, *Phys. Rev. D* **81** (2010) 036001 [[0908.2436](#)].
- [40] D. Suematsu, *Thermal Leptogenesis in a TeV Scale Model for Neutrino Masses*, *Eur. Phys. J. C* **72** (2012) 1951 [[1103.0857](#)].
- [41] D. Aristizabal Sierra, F. Bazzocchi and I. de Medeiros Varzielas, *Leptogenesis in flavor models with type I and II seesaws*, *Nucl. Phys. B* **858** (2012) 196 [[1112.1843](#)].
- [42] T. Hambye, *Leptogenesis: beyond the minimal type I seesaw scenario*, *New J. Phys.* **14** (2012) 125014 [[1212.2888](#)].
- [43] S. Kashiwase and D. Suematsu, *Leptogenesis and dark matter detection in a TeV scale neutrino mass model with inverted mass hierarchy*, *Eur. Phys. J. C* **73** (2013) 2484 [[1301.2087](#)].
- [44] D. Borah and M.K. Das, *Neutrino Masses and Leptogenesis in Type I and Type II Seesaw Models*, *Phys. Rev. D* **90** (2014) 015006 [[1303.1758](#)].
- [45] Y. Hamada and K. Kawana, *Reheating-era leptogenesis*, *Phys. Lett. B* **763** (2016) 388 [[1510.05186](#)].
- [46] Z.-h. Zhao, *Renormalization group evolution induced leptogenesis in the minimal seesaw model with the trimaximal mixing and mu-tau reflection symmetry*, *JHEP* **11** (2021) 170 [[2003.00654](#)].
- [47] S. Davidson, E. Nardi and Y. Nir, *Leptogenesis*, *Phys. Rept.* **466** (2008) 105 [[0802.2962](#)].
- [48] S. Blanchet and P. Di Bari, *The minimal scenario of leptogenesis*, *New J. Phys.* **14** (2012) 125012 [[1211.0512](#)].
- [49] N.S. Manton, *Topology in the Weinberg-Salam Theory*, *Phys. Rev. D* **28** (1983) 2019.
- [50] F.R. Klinkhamer and N.S. Manton, *A Saddle Point Solution in the Weinberg-Salam Theory*, *Phys. Rev. D* **30** (1984) 2212.
- [51] V.A. Kuzmin, V.A. Rubakov and M.E. Shaposhnikov, *On the Anomalous Electroweak Baryon Number Nonconservation in the Early Universe*, *Phys. Lett. B* **155** (1985) 36.
- [52] S.Y. Khlebnikov and M.E. Shaposhnikov, *The Statistical Theory of Anomalous Fermion Number Nonconservation*, *Nucl. Phys. B* **308** (1988) 885.
- [53] J.A. Harvey and M.S. Turner, *Cosmological Baryon and Lepton Number in the Presence of Electroweak Fermion Number Violation*, *Phys. Rev. D* **42** (1990) 3344.
- [54] S. Davidson and A. Ibarra, *A Lower bound on the right-handed neutrino mass from leptogenesis*, *Phys. Lett. B* **535** (2002) 25 [[hep-ph/0202239](#)].
- [55] M. Flanz, E.A. Paschos, U. Sarkar and J. Weiss, *Baryogenesis through mixing of heavy Majorana neutrinos*, *Phys. Lett. B* **389** (1996) 693 [[hep-ph/9607310](#)].
- [56] A. Pilaftsis, *Resonant CP violation induced by particle mixing in transition amplitudes*, *Nucl. Phys. B* **504** (1997) 61 [[hep-ph/9702393](#)].

- [57] A. Pilaftsis and T.E.J. Underwood, *Resonant leptogenesis*, *Nucl. Phys. B* **692** (2004) 303 [[hep-ph/0309342](#)].
- [58] B. Dev, M. Garny, J. Klaric, P. Millington and D. Teresi, *Resonant enhancement in leptogenesis*, *Int. J. Mod. Phys. A* **33** (2018) 1842003 [[1711.02863](#)].
- [59] I. Chakraborty, H. Roy and T. Srivastava, *Resonant leptogenesis in (2,2) inverse see-saw realisation*, *Nucl. Phys. B* **979** (2022) 115780 [[2106.08232](#)].
- [60] I. Chakraborty, H. Roy and T. Srivastava, *Searches for heavy neutrinos at multi-TeV muon collider: a resonant leptogenesis perspective*, *Eur. Phys. J. C* **83** (2023) 280 [[2206.07037](#)].
- [61] F.F. Deppisch, P.S. Bhupal Dev and A. Pilaftsis, *Neutrinos and Collider Physics*, *New J. Phys.* **17** (2015) 075019 [[1502.06541](#)].
- [62] Y. Cai, T. Han, T. Li and R. Ruiz, *Lepton Number Violation: Seesaw Models and Their Collider Tests*, *Front. in Phys.* **6** (2018) 40 [[1711.02180](#)].
- [63] A. de Gouvea and P. Vogel, *Lepton Flavor and Number Conservation, and Physics Beyond the Standard Model*, *Prog. Part. Nucl. Phys.* **71** (2013) 75 [[1303.4097](#)].
- [64] S. Alekhin et al., *A facility to Search for Hidden Particles at the CERN SPS: the SHiP physics case*, *Rept. Prog. Phys.* **79** (2016) 124201 [[1504.04855](#)].
- [65] G. Bertone, D. Hooper and J. Silk, *Particle dark matter: Evidence, candidates and constraints*, *Phys. Rept.* **405** (2005) 279 [[hep-ph/0404175](#)].
- [66] M. Cirelli, A. Strumia and J. Zupan, *Dark Matter*, [2406.01705](#).
- [67] PLANCK collaboration, *Planck 2018 results. VI. Cosmological parameters*, *Astron. Astrophys.* **641** (2020) A6 [[1807.06209](#)].
- [68] A. Liu, F.-L. Shao, Z.-L. Han, Y. Jin and H. Li, *Common origin of dark matter and leptogenesis in  $U(1)_{B-L}$* , *JHEP* **10** (2024) 019 [[2407.19730](#)].
- [69] R.E. Marshak and R.N. Mohapatra, *Quark - Lepton Symmetry and B-L as the  $U(1)$  Generator of the Electroweak Symmetry Group*, *Phys. Lett. B* **91** (1980) 222.
- [70] R.N. Mohapatra and R.E. Marshak, *Local B-L Symmetry of Electroweak Interactions, Majorana Neutrinos and Neutron Oscillations*, *Phys. Rev. Lett.* **44** (1980) 1316.
- [71] N. Okada and O. Seto, *Higgs portal dark matter in the minimal gauged  $U(1)_{B-L}$  model*, *Phys. Rev. D* **82** (2010) 023507 [[1002.2525](#)].
- [72] M. Escudero, N. Rius and V. Sanz, *Sterile neutrino portal to Dark Matter I: The  $U(1)_{B-L}$  case*, *JHEP* **02** (2017) 045 [[1606.01258](#)].
- [73] S. Okada,  *$Z'$  Portal Dark Matter in the Minimal B - L Model*, *Adv. High Energy Phys.* **2018** (2018) 5340935 [[1803.06793](#)].
- [74] S. Iso, N. Okada and Y. Orikasa, *Resonant Leptogenesis in the Minimal B-L Extended Standard Model at TeV*, *Phys. Rev. D* **83** (2011) 093011 [[1011.4769](#)].
- [75] J. Heeck and D. Teresi, *Leptogenesis and neutral gauge bosons*, *Phys. Rev. D* **94** (2016) 095024 [[1609.03594](#)].
- [76] P.S.B. Dev, R.N. Mohapatra and Y. Zhang, *Leptogenesis constraints on B - L breaking Higgs boson in TeV scale seesaw models*, *JHEP* **03** (2018) 122 [[1711.07634](#)].
- [77] T. Han, S. Li, S. Su, W. Su and Y. Wu, *Heavy Higgs bosons in 2HDM at a muon collider*, *Phys. Rev. D* **104** (2021) 055029 [[2102.08386](#)].

- [78] I. Esteban, M.C. Gonzalez-Garcia, M. Maltoni, I. Martinez-Soler, J.P. Pinheiro and T. Schwetz, *NuFit-6.0: updated global analysis of three-flavor neutrino oscillations*, *JHEP* **12** (2024) 216 [[2410.05380](#)].
- [79] MEG collaboration, *Search for the lepton flavour violating decay  $\mu^+ \rightarrow e^+\gamma$  with the full dataset of the MEG experiment*, *Eur. Phys. J. C* **76** (2016) 434 [[1605.05081](#)].
- [80] BABAR collaboration, *Searches for Lepton Flavor Violation in the Decays  $\tau^\pm \rightarrow e^\pm\gamma$  and  $\tau^\pm \rightarrow \mu^\pm\gamma$* , *Phys. Rev. Lett.* **104** (2010) 021802 [[0908.2381](#)].
- [81] M. Plumacher, *Baryogenesis and lepton number violation*, *Z. Phys. C* **74** (1997) 549 [[hep-ph/9604229](#)].
- [82] C.S. Fong, M.H. Rahat and S. Saad, *Low-scale resonant leptogenesis in  $SU(5)$  GUT with  $T_{13}$  family symmetry*, *Phys. Rev. D* **104** (2021) 095028 [[2103.14691](#)].
- [83] W. Buchmuller, P. Di Bari and M. Plumacher, *Leptogenesis for pedestrians*, *Annals Phys.* **315** (2005) 305 [[hep-ph/0401240](#)].
- [84] W. Buchmuller, P. Di Bari and M. Plumacher, *Cosmic microwave background, matter - antimatter asymmetry and neutrino masses*, *Nucl. Phys. B* **643** (2002) 367 [[hep-ph/0205349](#)].
- [85] G. Giudice, A. Notari, M. Raidal, A. Riotto and A. Strumia, *Towards a complete theory of thermal leptogenesis in the SM and MSSM*, *Nucl. Phys. B* **685** (2004) 89 [[hep-ph/0310123](#)].
- [86] I. Chakraborty and H. Roy, *Type-I thermal leptogenesis in  $Z_3$ -symmetric three Higgs doublet model*, *Eur. Phys. J. C* **80** (2020) 1038 [[1909.07790](#)].
- [87] M.H. Rahat, *Leptogenesis from the Asymmetric Texture*, *Phys. Rev. D* **103** (2021) 035011 [[2008.04204](#)].
- [88] M. Garny, A. Kartavtsev and A. Hohenegger, *Leptogenesis from first principles in the resonant regime*, *Annals Phys.* **328** (2013) 26 [[1112.6428](#)].
- [89] S. Iso, K. Shimada and M. Yamanaka, *Kadanoff-Baym approach to the thermal resonant leptogenesis*, *JHEP* **04** (2014) 062 [[1312.7680](#)].
- [90] S. Iso and K. Shimada, *Coherent Flavour Oscillation and CP Violating Parameter in Thermal Resonant Leptogenesis*, *JHEP* **08** (2014) 043 [[1404.4816](#)].
- [91] T. Hambye, *Leptogenesis at the TeV scale*, *Nucl. Phys. B* **633** (2002) 171 [[hep-ph/0111089](#)].
- [92] T. Hambye, J. March-Russell and S.M. West, *TeV scale resonant leptogenesis from supersymmetry breaking*, *JHEP* **07** (2004) 070 [[hep-ph/0403183](#)].
- [93] A. Pilaftsis, *Heavy Majorana neutrinos and baryogenesis*, *Int. J. Mod. Phys. A* **14** (1999) 1811 [[hep-ph/9812256](#)].
- [94] G.C. Branco, A.J. Buras, S. Jager, S. Uhlig and A. Weiler, *Another look at minimal lepton flavour violation,  $l_i \rightarrow l_j\gamma$ , leptogenesis, and the ratio  $M_\nu/\Lambda_{LFV}$* , *JHEP* **09** (2007) 004 [[hep-ph/0609067](#)].
- [95] V. Brdar, A.J. Helmboldt, S. Iwamoto and K. Schmitz, *Type-I Seesaw as the Common Origin of Neutrino Mass, Baryon Asymmetry, and the Electroweak Scale*, *Phys. Rev. D* **100** (2019) 075029 [[1905.12634](#)].
- [96] Y. Burnier, M. Laine and M. Shaposhnikov, *Baryon and lepton number violation rates across the electroweak crossover*, *JCAP* **02** (2006) 007 [[hep-ph/0511246](#)].

- [97] G. Bélanger, F. Boudjema, A. Goudelis, A. Pukhov and B. Zaldivar, *micrOMEGAs5.0 : Freeze-in*, *Comput. Phys. Commun.* **231** (2018) 173 [1801.03509].
- [98] LZ collaboration, *Dark Matter Search Results from 4.2 Tonne-Years of Exposure of the LUX-ZEPLIN (LZ) Experiment*, *Phys. Rev. Lett.* **135** (2025) 011802 [2410.17036].
- [99] D. Borah, A. Dasgupta and D. Mahanta, *TeV scale resonant leptogenesis with  $L_\mu - L_\tau$  gauge symmetry in light of the muon  $g - 2$* , *Phys. Rev. D* **104** (2021) 075006 [2106.14410].
- [100] ATLAS collaboration, *Search for high-mass dilepton resonances using  $139 \text{ fb}^{-1}$  of pp collision data collected at  $\sqrt{s} = 13 \text{ TeV}$  with the ATLAS detector*, *Phys. Lett. B* **796** (2019) 68 [1903.06248].
- [101] CMS collaboration, *Search for resonant and nonresonant new phenomena in high-mass dilepton final states at  $\sqrt{s} = 13 \text{ TeV}$* , *JHEP* **07** (2021) 208 [2103.02708].
- [102] S. Homiller, Q. Lu and M. Reece, *Complementary signals of lepton flavor violation at a high-energy muon collider*, *JHEP* **07** (2022) 036 [2203.08825].
- [103] D. Ally, L. Carpenter, T. Holmes, L. Lee and P. Wagenknecht, *Strategies for Beam-Induced Background Reduction at Muon Colliders*, in *Snowmass 2021*, 3, 2022 [2203.06773].
- [104] M. Antonelli, M. Boscolo, R. Di Nardo and P. Raimondi, *Novel proposal for a low emittance muon beam using positron beam on target*, *Nucl. Instrum. Meth. A* **807** (2016) 101 [1509.04454].
- [105] J. Alwall, R. Frederix, S. Frixione, V. Hirschi, F. Maltoni, O. Mattelaer et al., *The automated computation of tree-level and next-to-leading order differential cross sections, and their matching to parton shower simulations*, *JHEP* **07** (2014) 079 [1405.0301].
- [106] T. Sjöstrand, S. Ask, J.R. Christiansen, R. Corke, N. Desai, P. Ilten et al., *An introduction to PYTHIA 8.2*, *Comput. Phys. Commun.* **191** (2015) 159 [1410.3012].
- [107] C. Bierlich et al., *A comprehensive guide to the physics and usage of PYTHIA 8.3*, *SciPost Phys. Codeb.* **2022** (2022) 8 [2203.11601].
- [108] DELPHES 3 collaboration, *DELPHES 3, A modular framework for fast simulation of a generic collider experiment*, *JHEP* **02** (2014) 057 [1307.6346].
- [109] M. Boronat, J. Fuster, I. Garcia, P. Roloff, R. Simoniello and M. Vos, *Jet reconstruction at high-energy electron-positron colliders*, *Eur. Phys. J. C* **78** (2018) 144 [1607.05039].
- [110] M. Boronat, J. Fuster, I. Garcia, E. Ros and M. Vos, *A robust jet reconstruction algorithm for high-energy lepton colliders*, *Phys. Lett. B* **750** (2015) 95 [1404.4294].